THE ASTROPHYSICAL JOURNAL, 424:1032–1048, 1994 April 1

FOCUSED INTERPLANETARY TRANSPORT OF ~1 MeV SOLAR ENERGETIC PROTONS THROUGH SELF-GENERATED ALFVÉN WAVES

C. K. NG
Department of Mathematics, RMIT, Melbourne 3001, Victoria, Australia
AND
D. V. REAMES
Laboratory for High Energy Astrophysics, Code 661, NASA/Goddard Space Flight Center, Greenbelt, MD 20771
Received 1993 June 23; accepted 1993 October 5

ABSTRACT

We present a model of the focused transport of ~1 MeV solar energetic protons through interplanetary Alfvén waves that the protons themselves amplify or damp. It is based on the quasi-linear theory but with a phenomenological pitch angle diffusion coefficient in the "resonance gap." For initial Alfvén wave distributions that give mean free paths greater than ~0.5 AU for ~1 MeV protons in the inner heliosphere, the model predicts greater than roughly an order of magnitude amplification (damping) in the outward (inward) propagating resonant Alfvén waves at $\lesssim$0.3 AU heliocentric distance. As the strength of proton source is increased, the peak differential proton intensity at ~1 MeV at 1 AU increases to a maximum of ~250 particles (cm^2 s sr MeV)$^{-1}$ and then decreases slowly. It may be attenuated by a factor of 5 or more relative to the case without wave evolution, provided that the proton source is sufficiently intense that the resulting peak differential intensity of ~1 MeV protons at 1 AU exceeds ~200 particles (cm^2 s sr MeV)$^{-1}$.

Therefore, in large solar proton events, (1) one may have to take into account self-amplified waves in studying solar particle propagation, (2) the number of accelerated protons escaping from a flare or interplanetary shock may have been underestimated in past studies by a significant factor, and (3) accelerated protons escaping from a traveling interplanetary shock at $r \lesssim 0.3$ AU should amplify the ambient hydromagnetic waves significantly to make the shock an efficient accelerator, even if initially the mean free path is $\gtrsim$1 AU.

Subject headings: acceleration of particles — interplanetary medium — Sun: flares — Sun: particle emissions

1. INTRODUCTION

Wave-particle interaction is generally accepted as the cause of the scattering of solar energetic particles (SEP) in interplanetary space. In this view, low frequency hydromagnetic waves scatter the SEP and are in turn amplified or damped by the SEP. Nevertheless, a *time-independent* spatial mean free path or pitch diffusion coefficient has always been assumed in the analysis of observed solar particle events. If the SEP intensity is small, interplanetary hydromagnetic waves are probably not significantly modified by the passage of the SEP, and the test particle approach is valid. In large SEP events, however, can the waves be amplified to the extent that they significantly affect the propagation of the SEP themselves? It has been shown that wave generation plays a significant role for particle transport near shock waves and comets in the interplanetary medium (see, e.g., Lee 1982, 1983, 1988). In this paper, we study a simple time-dependent model of interplanetary SEP transport coupled to wave evolution, based on the quasi-linear theory modified by phenomenological scattering in the "resonance gap," and taking account of particle focusing by the interplanetary magnetic field.

The mean free path λ of SEP fitted using conventional models varies over 2 orders of magnitude from event to event (e.g., Palmer 1982; Wanner & Wibberenz 1993), and understanding the causes of this variability is an important current issue. A puzzling feature is the contrast between small and large SEP events (see, e.g., Reames 1992). For example, many small SEP events exhibit "scatter-free" propagation with very fast rise consistent with $\lambda \gtrsim 0.5$ AU (e.g., Mason et al. 1989). In contrast, large SEP events rise slowly to maximum (e.g., McCracken et al. 1971) and have been analyzed in the convection-diffusion model to give $\lambda \lesssim 0.1$ AU (see, e.g., Palmer 1982). Furthermore, there appears to be a limiting intensity early in the observed large SEP events (Reames 1990).

It is possible that the mean free path λ of MeV protons in the *undisturbed* interplanetary medium is often $\gtrsim$0.5 AU, and that the above difference is due to the modification of the interplanetary medium by the SEP themselves, or extended particle injection, or both. It is commonly believed that in *small impulsive* events, the SEP are accelerated in or near the flare and then released impulsively into interplanetary space. Cane, Reames, & von Rosenvinge (1988) argue that in *large gradual* events, a broad traveling interplanetary shock continuously accelerate the SEP, which subsequently escape from the shock (see also Lee & Ryan 1986). Large impulsive events have also been observed (Van Hollebeke, McDonald, & Meyer 1990) as well as events with the characteristics of both impulsive and gradual events. Small gradual events have not been reported; these are either nonexistent or below detection threshold.

We use the new model to explore SEP propagation over a range of particle source strength and initial distribution of interplanetary Alfvén waves, contrasting the results with those obtained in the absence of wave evolution. The present model does not include a traveling shock, which will be considered in a future paper. With reasonable initial interplanetary Alfvén wave distributions, proton source strength and other parameters, the model predicts that (1) for initial $\lambda \gtrsim 0.5$ AU, the resonant outward (inward) propagating Alfvén waves grow (decay) by an order of magnitude or more within a few hours at $r \lesssim 0.3$ AU, with the growth/decay rate increasing toward the

Sun, (2) as the proton source is increased, the maximum differential intensity of ~1 MeV proton at 1 AU rises to a maximum of ~250 particles $(cm^2\ s\ sr\ MeV)^{-1}$ and then slowly decreases, while the ratio between the maximum differential intensities calculated with and without wave growth decreases steadily from ≈ 1 to < 0.1, and (3) for initial $\lambda \gtrsim 0.5$ AU, the time-to-maximum at $r \lesssim 1$ AU is only slightly increased relative to the case without wave evolution, whereas for $\lambda \lesssim 0.2$ AU it is increased by a large factor.

This means that for the most intense particle events, the number of accelerated particles escaping from a solar flare or from a shock wave close to the Sun may have been underestimated in past studies by a significant factor. Even though consideration of a traveling shock together with its associated effects must be postponed to a future paper, the conclusion here means that accelerated protons escaping from the shock must excite enough waves to make the shock a very efficient accelerator, even if initially $\lambda > 0.5$ AU.

The idea of the amplification of hydromagnetic waves by streaming energetic particles and its influence on the propagation of the particles is not new. It was invoked in the context of the escape of cosmic rays from the galaxy (e.g., Tademaru 1969), particle acceleration associated with planetary bow shocks, traveling interplanetary shocks and comets (e.g., Lee 1982, 1983, 1988), and newly ionized interstellar neutrals (e.g., Wu & Davidson 1972; Lee & Ip 1987). In the context of SEP propagation, Reames (1989) suggested that in large solar proton events, the protons may excite interplanetary Alfvén waves significantly to affect their own propagation. Hydromagnetic wave excitation by interstellar hydrogen and helium ionized in the interplanetary medium has been modeled in the steady state or time asymptotics by Lee & Ip (1987). Pitch-angle diffusion of new-born ions was modeled by Yoon, Ziebell, & Wu (1991), taking into account resonant and nonresonant wave-particle interaction. This paper presents the first attempt to study SEP propagation using a time-dependent model coupling SEP propagation in the presence of magnetic focusing to Alfvén wave excitation/damping. Its novel features are the divergent radial geometry and the associated magnetic focusing of the particle pitch-angle distribution toward the anti-Sunward direction. The former implies that the peak differential intensity varies roughly as r^{-3}, and the latter that the particle distribution becomes more anisotropic with decreasing r (if scattering is weak). Together these lead to significant growth of the outward traveling Alfvén waves in the inner heliosphere.

The plan of the rest of this paper is as follows. In § 2, we detail the model assumptions, introduce the initial value problem consisting of the coupled partial differential equations governing the evolution of the particle and wave distributions, together with their initial and boundary conditions, and then describe their numerical solution. In § 3 we present, for a typical calculation, (1) the time histories of ~1 MeV proton differential intensity, anisotropy, and mean free path at 0.325, 0.525, and 1.125 AU, and (2) the evolution of the differential intensity of the various Alfvén wave modes at 0.325 AU, followed by (3) the dependence of the predictions on various model parameters. A discussion in § 4 closes the paper.

2. THE MODEL

2.1. *Assumptions and Equations*

Our model of the coupled evolution of solar energetic protons and interplanetary Alfvén waves is based on the quasi-linear theory (e.g., Lee 1971, 1982; Lee & Ip 1987) modified by phenomenological filling of the resonance gap. We make the following simplifying assumptions.

1. A radial mean interplanetary magnetic field (IMF). Although it is possible to use the Parker spiral field in modeling the focused transport of SEP (e.g., Ng & Wong 1979; Mason et al. 1989), we adopt the radial IMF here for simplicity and for consistency with our assumption of parallel propagating waves (see below). As wave growth decreases in relative importance with increasing heliocentric distance, this assumption is adequate for our purpose.
2. A radial solar wind velocity with constant speed.
3. The Alfvén speed varies inversely with heliocentric distance.
4. The IMF fluctuation is a superposition of *hydromagnetic* left- and right-hand circularly polarized transverse Alfvén waves propagating outward and inward *parallel* or *antiparallel* to the mean IMF. The actual IMF fluctuation includes other wave modes of relevance to the SEP, e.g., obliquely propagating Alfvén waves, magnetosonic and ion cyclotron waves. Including these will introduce further complexity and is not attempted in the present model.
5. The SEP consist of energetic protons only. We adopt this assumption for simplicity, even though the SEP include a significant fraction of energetic He^{++} and other ions. The model predictions should not be significantly affected by this assumption.
6. The energetic protons are injected at 0.1 AU helioradius, are focused by the mean IMF and scattered by the interplanetary Alfvén waves through cyclotron resonance according to the quasi-linear theory.
7. Correspondingly the Alfvén waves are either amplified or damped by the energetic protons.
8. For parallel and antiparallel hydromagnetic Alfvén waves with a upper cutoff wave number, the quasi-linear theory gives a resonance gap in pitch angle space in which the pitch diffusion coefficient is zero. Observation, however, indicates that the SEP are scattered over all pitch angles, and that there are no transport gap in pitch angle space. It is beyond the scope of this paper to take into account nonresonant scattering and nonlinear theories which allow the SEP to traverse the gap. Instead we adopt a phenomenological approach and fill in the gap with the average of the pitch diffusion coefficient just outside the gap.
9. We consider only induced emission and absorption, and ignore spontaneous emission and absorption, mode-mode coupling, and nonlinear damping of Alfvén waves (e.g., Melrose 1980; Miller 1991).
10. For simplicity, we ignore particle momentum transport required by the quasi-linear theory, i.e., we ignore the terms associated with the coefficients $D_{\mu p}$ and D_{pp} in the transport equation (e.g., Schlickeiser 1989a, b). The model is thus not self-consistent as regards energy conservation. However, momentum diffusion proceeds slower than pitch diffusion by a factor $\approx V_A/v$, which reaches a maximum of only $\approx 2.5 \times 10^{-2}$ for 45 MV protons in the model.
11. Wave propagation is ignored as we are mainly interested in a timescale of ≈ 10 hr.

We shall use the following notation: t = time, $\boldsymbol{r}$ = heliocentric radius vector, $\hat{\boldsymbol{r}}$ = unit radial vector, $\boldsymbol{p}$ = particle momentum, c = speed of light, e = elementary charge, $\boldsymbol{P} = \boldsymbol{p}c/e$ = proton rigidity, m_p = proton mass, $\mathscr{E}_0 = m_p c^2$ = proton rest energy, $\mathscr{E}$ = proton total energy, r_0 = reference

radius = 1 AU, $\boldsymbol{B} = B\hat{\boldsymbol{r}} = B_0(r_0/r)^2\hat{\boldsymbol{r}}$ = mean interplanetary magnetic field, $\boldsymbol{v}$ = particle velocity, $\mu = \boldsymbol{v}\cdot\hat{\boldsymbol{r}}/v$ = particle pitch, $f(P, \mu, r, t)$ = density of solar protons in $(\boldsymbol{P}, \boldsymbol{r})$ space averaged over gyrophase, $D_{\mu\mu}(P, \mu, r, t)$ = particle diffusion coefficient in μ-space, λ = particle mean free path, V = solar-wind speed, $V_A = V_{A0}(r_0/r)$ = Alfvén speed, $V_\pm = V \pm V_A$ = phase speed of outward (inward) traveling Alfvén waves, $\Omega = ecB/\mathscr{E}$ = (signed) proton gyrofrequency, ω = angular frequency of Alfvén wave, k = (parallel) wave number, h = wave helicity label, σ = wave polarization label, d = label for wave propagation direction in plasma frame, $I_d(k, r, t)$ = differential intensities of the magnetic field fluctuation of circularly polarized outward and inward propagating Alfvén waves, with $d = \pm$ denoting outward (inward) propagation relative to the plasma, and $k \lesseqgtr 0$ denoting left (right) helicity. We also define the differential wave intensities associated with Alfvén waves of left- and right-helicity: $I_d^L(k, r, t) = I_d(k, r, t)$, for $k > 0$, and $I_d^R(|k|, r, t) = I_d(k, r, t)$, for $k < 0$. The differential wave intensities are normalized such that

$$\langle \delta\boldsymbol{B}\cdot\delta\boldsymbol{B}\rangle = \sum_{d=\pm}\int_{-\infty}^{\infty} dk I_d(k, r, t) = \sum_{d=\pm}\sum_{h=L,R}\int_0^\infty d\zeta I_d^h(\zeta, r, t)\,, \tag{1}$$

where $\delta\boldsymbol{B}$ = fluctuating magnetic field, and angle brackets denote ensemble average. Finally, $\gamma_d^h(\zeta, r, t)$ = growth rate of $I_d^h(\zeta, r, t)$.

In the *fixed inertial frame*, the evolution of the proton phase space density averaged over gyrophase is governed by the focused transport equation (Roelof 1969)

$$\frac{\partial f}{\partial t} + \mu v\frac{\partial f}{\partial r} + \frac{1-\mu^2}{r}v\frac{\partial f}{\partial \mu} = \frac{\partial}{\partial\mu}\left(D_{\mu\mu}\frac{\partial f}{\partial\mu}\right), \tag{2}$$

where the third term on the left is due to focusing by the radial IMF, and the term on the right describes diffusion in μ-space due to scattering by the Alfvén waves. In equation (2), the pitch diffusion coefficient $D_{\mu\mu}(P, \mu, r, t)$ is expressed according to the quasi-linear theory in terms of the differential wave intensities $I_d^h(|k|, r, t)$ evaluated at the resonant wavenumbers $|k_\pm^{res}|$ (e.g., Schlickeiser 1989b):

$$D_{\mu\mu}(P, \mu, r, t) = \frac{\pi}{2}\left(\frac{\Omega}{B}\right)^2(1-\mu^2) \times [Q_+ I_+^\alpha(|k_+^{res}|, r, t) + Q_- I_-^\beta(|k_-^{res}|, r, t)]\,, \tag{3}$$

$$Q_\pm = (1 - \mu V_\pm/v)^2/|\mu v - V_\pm|\,, \tag{4}$$

$$k_\pm^{res} = \Omega/(\mu v - V_\pm) = B/[P(\mu - V_\pm/v)]\,. \tag{5}$$

For $B > 0$ (<0), the helicity indices α and β are chosen as follows:

$$\alpha = \begin{cases} \text{L(R)} & \text{if } \mu v > V_+\,, \\ \text{R(L)} & \text{otherwise}\,, \end{cases} \tag{6}$$

$$\beta = \begin{cases} \text{R(L)} & \text{if } \mu v < V_-, \\ \text{L(R)} & \text{otherwise}\,. \end{cases} \tag{7}$$

The resonant wavenumbers $k_\pm^{res}$ in equation (5) are obtained by eliminating ω between the dispersion relation for Alfvén waves,

$$\omega = k(V \pm V_A)\,, \tag{8}$$

valid for $|\omega - kV| = |kV_A| \ll |\Omega|$, and the condition for cyclotron resonance

$$\omega - k\mu v + \Omega = 0\,. \tag{9}$$

We follow the convention of, e.g., Lee & Ip (1987), so that $\omega > 0$ corresponds to right-hand (left-hand) polarization if $B > 0$ (<0). In Table 1 we summarize the relationships among the wavenumber k, the helicity h, which are both Galilean invariant, and the propagation direction relative to the plasma d, the wave frequency ω, the polarization σ, and a necessary condition on μv derived from equation (5) for the SEP to resonate with the wave, in both the plasma and the "spacecraft" frame. We work mainly with k (or $|k|$) and h, because these are Galilean invariant, rather than with ω and σ, which are frame dependent.

The choice of α and β in equations (6) and (7) is based on the fact that, for $B > 0$ ($B < 0$), protons streaming outward gyrate in the left (right) hand sense, and thus can only resonate with Alfvén waves of left (right) helicity, provided their parallel velocities exceed the local phase velocities of the Alfvén waves (Table 1). Similar consideration applies for inward-streaming protons.

Restriction to parallel hydromagnetic waves with a cutoff frequency below the proton gyrofrequency results in a resonance gap in μ-space according to the quasi-linear theory (eqs. [3] and [5]). However, other waves (e.g., oblique Alfvén waves, magnetosonic waves, and ion cyclotron waves) do scatter the protons in at least a portion of the gap. Furthermore, there is no doubt that particles do diffuse across the gap, and nonlinear theories, such as resonance broadening have been invoked to explain this fact (e.g., Völk 1973, 1975; Jones, Kaiser, & Birmingham 1973; Goldstein 1976; Yoon et al. 1991; Karimabadi, Krauss-Varban, & Terasawa 1992). Inclusion of other wave modes and a self-consistent treatment of resonance broadening are beyond the scope of this paper, and we simply "fill in" the gap phenomenologically with the average of the values of $D_{\mu\mu}$ just outside the gap (see below).

As we are concerned with a time duration $\sim$10 hr and $V + V_A$ is $\lesssim 2\times10^{-2}$ AU hr^{-1}, we ignore wave propagation. Considering only stimulated emission and absorption, we approximate the evolution of the differential wave intensities *in the fixed inertial frame* by the equation

$$\frac{\partial I_d^h(|k|, r, t)}{\partial t} = \gamma_d^h(|k|, r, t) I_d^h(|k|, r, t)\,, \quad (h = \text{L, R};\quad d = \pm)\,, \tag{10}$$

TABLE 1

ALFVÉN WAVE DESCRIPTIONS

		Plasma Frame				Spacecraft Frame		
k	h	d	ω	σ	Condition[a]	ω	σ	Condition[a]
					Case $B > 0$			
+	L	+	+	R	$\mu v > V_A$	+	R	$\mu v > V + V_A$
+	L	−	−	L	$\mu v > -V_A$	+	R	$\mu v > V - V_A$
−	R	−	+	R	$\mu v < -V_A$	−	L	$\mu v < V - V_A$
−	R	+	−	L	$\mu v < V_A$	−	L	$\mu v < V + V_A$
					Case $B < 0$			
+	L	+	+	L	$\mu v < V_A$	+	L	$\mu v < V + V_A$
+	L	−	−	R	$\mu v < -V_A$	+	L	$\mu v < V - V_A$
−	R	−	+	L	$\mu v > -V_A$	−	R	$\mu v > V - V_A$
−	R	+	−	R	$\mu v > V_A$	−	R	$\mu v > V + V_A$

[a] A necessary condition for cyclotron resonance.

where

$$\gamma_{\pm}^{h}(|k|, r, t) = \pm \frac{4\pi^3 e V_A}{|k|c} \int d\mu \times \left\{ \frac{(1-\mu^2)vP^2}{|\mu - vV_{\pm}/c^2|} \left[\frac{\partial f}{\partial \mu} - \frac{V_{\pm}}{v} \left(\mu \frac{\partial f}{\partial \mu} - P \frac{\partial f}{\partial P} \right) \right] \right\}_{P_{res}}, \quad (11)$$

(e.g., Lee 1972, 1982; Melrose 1980). For $B > 0$ (< 0), the integral is evaluated over the interval $(V_{\pm}/c, 1]$ for $h = \mathrm{L(R)}$, and the interval $[-1, V_{\pm}/c)$ for $h = \mathrm{R(L)}$. The integrand is evaluated at the resonant rigidity P_{res} given below. By using the dispersion relation (8) for the Alfvén waves and the condition (9) for cyclotron resonance, we find for the waves with $k/B \gtrless 0$, the resonant proton rigidities (necessarily at $\mu \gtrless V_{\pm}/c$):

$$P_{res} = \frac{B}{k(\mu^2 - V_{\pm}^2/c^2)} \left[\mu + \frac{V_{\pm}}{c} \sqrt{1 + \left(\mu^2 - \frac{V_{\pm}^2}{c^2} \right) \left(\frac{k\mathscr{E}_0}{eB} \right)^2} \right]. \quad (12)$$

Note that $|(V_A/c)(k\mathscr{E}_0/eB)| = |(\omega - kV)/\Omega| \ll 1$ for hydromagnetic waves.

From equation (11), we see that irrespective of the sign of B, a positive value of $\partial f/\partial \mu$ simultaneously contributes to the growth of the outward Alfvén waves and the decay of the inward Alfvén waves. "Outward" moving protons with $\partial f/\partial \mu > 0$ at $\mu > (V \pm V_A)/v$ amplify outward right-hand polarized Alfvén waves, and damp inward left-hand polarized Alfvén waves, polarization here being referred to the plasma frame (Stix 1962) (in the fixed frame, both waves are right-hand polarized; see Table 1). Similarly, "inward" moving protons with $\partial f/\partial \mu > 0$ at $\mu < (V \pm V_A)/v$ amplify outward left-hand polarized Alfvén waves and damp inward right-hand polarized Alfvén waves, polarization here being referred to the plasma frame (both waves are left-hand polarized in the fixed frame). If $\partial f/\partial \mu < 0$, the above contributions towards amplification or damping are reversed. In the early phase of a solar particle event, we usually have $\partial f/\partial \mu > 0$. The last term in the integral in equation (11) vanishes in the rest frame of the corresponding wave mode, and so a particle distribution that is isotropic in that frame does not excite or damp that wave mode. This last term has often been interpreted as a threshold that $\partial f/\partial \mu$ must exceed in order to excite waves traveling in the direction of the particles as seen in the plasma rest frame. This is so if $\partial f/\partial P < 0$. In the onset phase of a solar particle event, however, $\partial f/\partial P$ is positive because of velocity dispersion and contributes to wave growth. Equation (11) applies strictly for a constant mean magnetic field. However, provided the relevant wave lengths are much smaller than the magnetic focusing length, it should be a reasonable approximation.

For numerical solution it is preferable to write the focused transport equation in conservation form. This may be done in general by using f/B instead of f. As we have assumed $B = B_0(r_0/r)^2$, we introduce

$$F(P, \mu, r, t) = (r/r_0)^2 f(P, \mu, r, t), \quad (13)$$

and rewrite the focused particle transport equation (2) in the conservation form

$$\frac{\partial F}{\partial t} + \frac{\partial}{\partial r}(\mu v F) + \frac{\partial}{\partial \mu}\left(\frac{1-\mu^2}{r} v F \right) = \frac{\partial}{\partial \mu}\left(D_{\mu\mu} \frac{\partial F}{\partial \mu} \right). \quad (14)$$

The resonant wavenumber k_{res} varies strongly with helioradius r through its dependence on B (see eq. [5]). This strong dependence on r may be avoided if we used the normalized wavenumber $\eta = |k/B|$ (with dimension of inverse rigidity) instead of $|k|$, and redefine $I_d^h = I_d^h(\eta, r, t)$ and $\gamma_d^h = \gamma_d^h(\eta, r, t)$. From equation (5) we have the normalized resonant wavenumber

$$\eta_{\pm}^{res} = (P|\mu - V_{\pm}/v|)^{-1}. \quad (15)$$

and the pitch diffusion coefficient

$$D_{\mu\mu}(P, \mu, r, t) = \frac{\pi}{2}\left(\frac{\Omega}{B} \right)^2 (1-\mu^2) \times [Q_+ I_+^{\alpha}(\eta_+^{res}, r, t) + Q_- I_-^{\beta}(\eta_-^{res}, r, t)], \quad (16)$$

with $Q_{\pm}$, α, and β again given by equations (4), (6), and (7), respectively, and modified by resonance broadening as described previously. Equations (10) and (11) governing wave evolution now read

$$\frac{\partial I_d^h(\eta, r, t)}{\partial t} = \gamma_d^h(\eta, r, t) I_d^h(\eta, r, t), \quad (h = L, R; \quad d = \pm), \quad (17)$$

$$\gamma_{\pm}^{h}(\eta, r, t) = \pm \frac{4\pi^3 e V_A}{\eta c |B_0|} \int d\mu \times \left\{ \frac{(1-\mu^2)vP^2}{|\mu - vV_{\pm}/c^2|} \left[\frac{\partial F}{\partial \mu} - \frac{V_{\pm}}{v}\left(\mu \frac{\partial F}{\partial \mu} - P \frac{\partial F}{\partial P} \right) \right] \right\}_{P_{res}}, \quad (18)$$

Equations (14) and (17) form a set of partial differential equations for the evolution of the particle and wave distributions coupled via equations (16) and (18). We shall consider these equations in the following domain: 0.1 AU $\leq r \leq$ 2.6 AU, 16 MV $\leq P \leq$ 107.6 MV, $-1 \leq \mu \leq 1$, and 9.716×10^{-3} MV^{-1} $\leq \eta \leq 3.447 \times 10^{-1}$ MV^{-1}. The model is specified by the initial value problem consisting of the above equations and suitable initial and boundary conditions on the particle and wave distributions.

2.2. *Initial and Boundary Conditions*

2.2.1. *Initial Proton Distribution*

If the background energetic particle distributions are in equilibrium with the interplanetary Alfvén waves, then their contribution to the wave growth rate in equation (18) is zero. If the background is due to the "quiet time" background and not to a recent solar particle event (which is not considered in this paper), we believe this to be the case. The observed quiet time differential intensity of low-energy interplanetary ions at ~1 AU is $j_{\mathscr{E}} \lesssim 0.1$ (cm^2 s sr MeV amu^{-1})$^{-1}$ at ~1 MeV amu^{-1} and nearly isotropic with a spectral index in the range of -2.5 to -3.1. (Richardson et al. 1990). This is small compared to the observed peak differential intensity ~10–500 (cm^2 s sr MeV)$^{-1}$ of SEP at ~1 MeV. The peak differential intensity of SEP should rise steeply toward the Sun, roughly like r^{-3}, and should thus dominate the background intensity even more in the inner heliosphere, where wave excitation is found to be important. In view of the above we employ an initial proton distribution that is either identically zero or based on the above quiet time background and independent of r.

2.2.2. *Outer Boundary Condition on the Protons*

We stipulate a free-escape boundary condition at $r = 2.6$ AU. A ~1 MeV proton would take a total of ≈12 hr to travel from the Sun to $r = 2.6$ AU at $\mu = 1$ and thence back to $r = 1$ AU at $\mu = -1$. In the presence of scattering, the average time for such a trip is longer by a factor greater than 2 (Earl 1974).

Thus the effect of the outer boundary on the calculated particle and wave intensities at $r \lesssim 1$ AU and $t \lesssim 10$ hr is insignificant.

2.2.3. *Inner Boundary Condition on the Protons*

The injection of protons is specified via a time-dependent source $S(P, \mu, r, t)$ at the inner spatial boundary $r = r_0$, at which protons with $\mu < 0$ are also reflected, viz.,

$$f(P, \mu, r_0, t) = S(P, \mu, r_0, t) + f(P, -\mu, r_0, t), \quad (\mu > 0). \quad (19)$$

We employ a separable function for the source term,

$$S(P, \mu, r_0, t) = \mathcal{I}(P)\mathcal{M}(\mu)\mathcal{T}(t). \quad (20)$$

Clearly, one can specify the function S in many ways. For simplicity, we limit ourselves to only a few forms. We use $\mathcal{M}(\mu) = H(\mu)$ and $\mathcal{M}(\mu) = \mu H(\mu)$, with $H(\mu)$ the Heaviside step function, to study the effect of varying the μ-dependence of the source. We use an exponentially decaying source, $\mathcal{T}(t) = \exp(-t/t_{\rm inj})$, and study the effect of varying the injection time constant $t_{\rm inj}$. We adopt

$$\mathcal{I}(P) = j_{\mathcal{E}}^0 \frac{ev_0}{cvP^2} \exp\left[-\frac{P}{P_1} - \left(\frac{P_2}{P}\right)^2 + \frac{P_0}{P_1} + \left(\frac{P_2}{P_0}\right)^2 \right], \quad (21)$$

in which the spectral shape is specified by the parameters P_1 and P_2, and the injection strength is specified by the parameter $j_{\mathcal{E}}^0$, which is the source differential intensity with respect to energy at the reference rigidity P_0, $\mu = 1$, $r = r_0$, and $t = 0$. The quantity v_0 is the proton speed corresponding to the rigidity P_0. Note that at $P = P_0$, the argument of the exponential function vanishes and equation (21) gives $(c/e)P_0^2\mathcal{I}(P_0) = j_{\mathcal{E}}^0$.

Ideally the proton injection rigidity spectrum should be consistent with the observed time-of-maximum spectrum (e.g., McGuire, von Rosenvinge, & McDonald 1981; McGuire & Rosenvinge 1984; Reames, Richardson, & Wenzel 1992), or with the theoretical predictions of acceleration models, e.g., the Bessel-function spectrum of M. A. Lee reported in Forman, Ramaty, & Zweibel (1986). However, our numerical model is necessarily restricted to a finite range of proton rigidity roughly centered at 43.33 MV, the rigidity of the 1 MeV protons of interest here. In this paper, we generally adopt $P_0 = 43.33$ MV, $P_1 = 25$ MV, and $P_2 = 21.6$ MV, and study the effect of the source strength by varying $j_{\mathcal{E}}^0$. This spectrum of $\mathcal{I}$ decreases monotonically in $(P_L, P_U) = (16$ MV, 107.6 MV), and steepens as P increases such that at $P \gg P_2$, $vP^2\mathcal{I} \propto \exp(-P/P_1)$. As a function of energy, $P^2\mathcal{I}$ peaks at $\sim$260 keV (22 MV), and the energy spectral index $\partial \log (P^2\mathcal{I})/\partial \log \mathcal{E}$ decreases from 1 at 136 keV (16 MV) to -1.1 at 1 MeV (43 MV), consistent with observation, and steepening to -2.6 at 6 MeV (107 MV). Finally, the effect of the spectral shape is studied by varying P_1 and P_2 (see § 3.8).

With the exponentially decaying source, the same total number of particles are injected over the time interval $(0, \infty)$ if the constants $j_{\mathcal{E}}^0$ and $t_{\rm inj}$ are chosen such that $j_{\mathcal{E}}^0 t_{\rm inj} =$ constant. However, with small $t_{\rm inj}$ and large $j_{\mathcal{E}}^0$, the large proton intensity near the inner spatial boundary at early time produces large wave growth/decay rates, thus imposing severe requirement on the computational time step in the numerical model. Hence we adopt $t_{\rm inj} \geq 1$ hr in most of our calculations.

2.2.4. *Rigidity and Wavenumber Boundaries*

We are interested mainly in $P \sim 43$ MV (i.e., 1 MeV) protons, for which the normalized resonant Alfvén wavenumber $\eta_{\rm res}$ ranges from $(P|1 \pm V_\pm/v|)^{-1}$ at $\mu = \mp 1$ to very large values as $\mu \to V_\pm/v$ (eq. [15]). On the other hand, any of these Alfvén waves resonates with protons of a minimum rigidity at $\mu \approx \pm 1$ to infinite rigidity as $\mu \to V_\pm$ (eq. [12]). This is clearly a global issue: protons of different rigidities and pitch angles are coupled via interaction with the same Alfvén waves, and this equires that we consider infinite ranges of particle rigidities and wavenumbers. However, practicality requires that we consider only finite ranges, and equations (12) and (15) are only valid for hydromagnetic waves anyway. So, for simplicity, we confine ourselves to these waves and set the upper η-boundary at $\eta_U = \alpha|\Omega/BV_{\rm A}|_{\rm min}$, with $\alpha \approx 0.4$ and "min" denoting the minimum value on the spatial grid (actually the assumption of hydromagnetic waves require $\alpha \ll 1$). For example, with $V_{\rm A0} = 1 \times 10^{-3}$ AU hr^{-1}, we set $\eta_U = 0.3447$ MV^{-1} [actually the effective cutoff is at $\eta_U\, 10^{(1/2)\Delta(\log_{10}\eta)}$].

The high cutoff η_U implies a resonance gap in μ given by $V_+/v - 1/(P\eta_U) < \mu < V_-/v + 1/(P\eta_U)$, in which $D_{\mu\mu} = 0$. However, as noted earlier, the presence of other wave modes and nonlinear theories allow the protons to diffuse across the gap, and we "fill in" the gap with the average of the values of $D_{\mu\mu}$ just outside the gap. Because $I_-^{\rm L}$ and $I_-^{\rm R}$ contribute negligibly to particle scattering compared to $I_+^{\rm L}$ and $I_+^{\rm R}$, we also approximate the gap by $V_+/v - 1/(P\eta_U) < \mu < V_+/v + 1/(P\eta_U)$.

For $\eta_U = 0.3447$ MV^{-1}, the minimum value of $P_{\rm res}$ is 5.365 MV. However, it is not practical to choose the latter as the value of the lower rigidity boundary $P_{\rm L}$, because 5.365 MV protons with $|\mu| < 0.8$ do not resonate with hydromagnetic waves with $\eta < \eta_U$. As P decreases, the μ-range for resonance with hydromagnetic waves shrinks, leading presumably to faster leveling of the proton pitch distribution in that μ-range, and smaller contribution to hydromagnetic wave growth. In view of the above we choose $P_L = 16$ MV. Furthermore, since protons with $P < 16$ MV take more than $\sim$3 times longer than 43 MV protons to travel to any location to amplify or damp the waves there, neglecting these low-energy protons will not have any effect on the 43 MV proton differential intensity until long after the intensity peak.

We adopt an upper rigidity boundary at $P_U \approx 107.6$ MV. It is computationally expensive to choose a large value for P_U, as high proton velocity requires small computational time step in the numerical model. In equation (18), the integrand decreases quickly with rigidity, and we take approximate account of the contribution of higher rigidity protons by extrapolating F with, e.g., a P^{-8} spectrum beyond P_U. This smooths and raises somewhat the wave intensity spectra at low wave numbers. Protons at $P = P_U$ and $\mu = 0.95$ have the lowest $\eta_{\rm res}$, which is just larger than 0.0095 MV^{-1}. Hence we choose η_L so that the effective cutoff $\eta_L\, 10^{-(1/2)\Delta(\log_{10}\eta)}$ is below 0.0095 MV^{-1}.

Finally it is convenient to use logarithmic scales for P and η. The $\ln P$ interval is chosen as $(\ln 16, \ln 107.6)$ with step size $\Delta(\ln P) = 0.08664$ and P in MV. The $\log_{10}\eta$ interval is chosen as $(-2.0125, -0.4625)$, with step size $\Delta(\log_{10}\eta) = 0.05$.

2.2.5. *Initial Conditions on the Alfvén Waves*

In contrast to the initial background particle intensity, the initial differential wave intensities specify $D_{\mu\mu}$ and set the stage for the initial scattering of the SEP, and so play a significant role in the subsequent evolution of the particle and wave distributions.

The observed power spectrum of IMF fluctuation within 1 AU is roughly a power law k^δ above some critical wavenumber with $\delta \approx -1.5$, and varies with heliocentric distance approx-

imately as r^{-3} (Bavassano et al. 1982; Marsch & Tu 1990; Roberts, Goldstein, & Klein 1990). It appears to be mainly Alfvénic in nature, with most of the power (>90%) in the outward propagating waves (Denskat & Neubauer 1982). The observed radial variation at $r \lesssim 1$ AU is roughly in agreement with the predictions of the WKB theory (e.g., Whang 1973; Hollweg 1974).

The nature of IMF fluctuation and its radial evolution is a complex issue (e.g., Tu, Pu, & Wei 1984; Roberts & Goldstein 1991; Marsch 1991; Bruno & Bavassano 1991), and is not the concern of this paper. Our purpose is to investigate the excitation of a preexisting wave distribution by streaming SEP, and the back influence of the excited waves on SEP propagation. To this end we only need to specify an initial wave intensity distribution reasonably consistent with the observation. Here we specify the initial differential outward wave intensities I^h_+ via steady state solutions of the wave transport equation. We assume equal differential intensities for the two outward waves, $I^L_+ = I^R_+$, and set the initial differential intensities of the inward waves at 10% of that of the outward waves, i.e., $I^L_- = I^R_- = 0.1 I^L_+$.

The wave transport equation for $\mathscr{W}^h_+(\boldsymbol{k}, \boldsymbol{r}, t)$, the *total* wave energy density in phase space, is (e.g., Barnes 1979)

$$\frac{\partial \mathscr{W}^h_+}{\partial t} + \frac{\partial \omega}{\partial \boldsymbol{k}} \cdot \frac{\partial \mathscr{W}^h_+}{\partial \boldsymbol{r}} - \frac{\partial \omega}{\partial \boldsymbol{r}} \cdot \frac{\partial \mathscr{W}^h_+}{\partial \boldsymbol{k}} = \gamma \mathscr{W}^h_+ \,. \tag{22}$$

If we assume a radial IMF, solar wind velocity $V(r)\hat{\boldsymbol{r}}$, Alfvén velocity $V_A(r)\hat{\boldsymbol{r}}$, dispersion relation for Alfvén waves $\omega = \boldsymbol{\kappa} \cdot [(V + V_A)\hat{\boldsymbol{r}}]$, and set

$$\mathscr{W}^h_+(\boldsymbol{k}, \boldsymbol{r}, t) = \frac{W^h_+(k, r, \theta, \phi, t)}{k^2 \sin \theta_k} \delta(\theta_k - \theta)\delta(\phi_k - \phi) \,, \tag{23}$$

where (r, θ, ϕ) are the spatial spherical coordinates, and (k, θ_k, ϕ_k) are the spherical coordinates in $\boldsymbol{k}$-space, then equation (22) may be manipulated into

$$\frac{\partial W^h_+}{\partial t} + \frac{1}{r^2}\frac{\partial}{\partial r}(r^2 V_g W^h_+) - \frac{\partial}{\partial k}\left(k \frac{\partial V_g}{\partial r} W^h_+\right) = \gamma W^h_+ \,, \tag{24}$$

where $V_g(r) = V(r) + V_A(r)$. If we set $\partial/\partial t \equiv 0$, $\gamma \equiv$ constant, and impose a power-law spectra at the reference radius r_0:

$$W^h_+(k, r_0, \theta, \phi) = W^h_{+0}(\theta, \phi)(k/k_0)^\delta \,, \quad (h = \mathrm{L}, \mathrm{R}) \,, \tag{25}$$

where k_0 is a reference wavenumber, then the steady state solution of equation (24), subject to the boundary condition (25) at $r = r_0$, is given by

$$W^h_+(k, r) = W^h_{+0}\left(\frac{r_0}{r}\right)^2 \left[\frac{k}{k_0}\frac{V(r) + V_A(r)}{V(r_0) + V_A(r_0)}\right]^\delta \times \exp\left[\gamma \int_{r_0}^{r} \frac{dr}{V(r) + V_A(r)}\right], \tag{26}$$

where we have omitted the parametric dependence on θ and ϕ for clarity. Following Barnes (1979), we transform $W^h_+(k, r)$ in equation (26) from the fixed inertial frame to the plasma frame, in which the energy density of magnetic fluctuation is approximately half the total energy density of the Alfvén waves. Thus we obtain the differential intensities of *magnetic* fluctuations of the Alfvén waves

$$I^h_+(k, r) = I^h_{+0}\left(\frac{k}{k_0}\right)^\delta \frac{r_0^2 V_A(r)}{r^2 V_A(r_0)} \left[\frac{V(r) + V_A(r)}{V(r_0) + V_A(r_0)}\right]^{\delta - 1} \times \exp\left(\gamma \int_{r_0}^{r} \frac{dr}{V + V_A}\right). \tag{27}$$

where I^h_{+0} are the differential outward wave intensities at the reference wavenumber k_0 and reference radius $r_0 = 1$ AU. For $\gamma = 0$, $V_A = V_{A0}(r_0/r)$, and $V > V_A$, equation (27) implies that I^h_+ at constant k varies approximately as r^{-3}, in rough agreement with observations and the prediction of WKB theory. For example, it is in agreement with the solution of Tu et al. (1984) specialized to the situation without cascading effects (i.e., their eq. [54] at $f \gg f_c$ with $\alpha = 0$.)

Let us consider waves in the wavenumber interval $[k(r_0), k(r_0) + dk(r_0)]$ at $r = r_0$. The rays of these waves are governed by $d\boldsymbol{r}/dt = \partial\omega/\partial\boldsymbol{k}$, and $d\boldsymbol{k}/dt = -\partial\omega/\partial\boldsymbol{r}$. Hence along the rays

$$k(r) = k(r_0)[V(r_0) + V_A(r_0)]/[V(r) + V_A(r)] \,, \tag{28}$$

$$dk(r) = dk(r_0)[V(r_0) + V_A(r_0)]/[V(r) + V_A(r)] \,. \tag{29}$$

From equations (27)–(29), we obtain the variation of the intensity of these waves along the rays:

$$I^h_+[k(r), r]dk(r) = I^h_{+0}\, dk(r_0) \frac{r_0^2 V_A}{r^2 V_{A0}} \left[\frac{V(r_0) + V_A(r_0)}{V(r) + V_A(r)}\right]^2 \times \exp\left(\gamma \int_{r_0}^{r} \frac{dr}{V + V_A}\right). \tag{30}$$

With $\gamma = 0$, $\boldsymbol{k}$ parallel or antiparallel to $\boldsymbol{B}$, and $k(r)$ given by equation (28), this result is in agreement with equation (26) of Barnes (1992), and equation (23) of Hollweg (1974).

Since $k_{\mathrm{res}} \propto r^{-2}$ (see eq. [5]), and the outward waves dominate, the differential wave intensity distribution in equation (27) with $\gamma = 0$ implies that $D_{\mu\mu}$ in equation (3) is roughly $\propto r^{-3-2\delta}(V + V_A)^{-1}$, or $\lambda \propto r^{3+2\delta}(V + V_A)^{1-\delta}$. For $\delta = -5/3$ (Kolmogorov spectrum), this means the particle mean free path λ is roughly $\propto r^{-1/3}(V + V_A)^{8/3}$, decreasing by a factor of ≈ 10 when r is increased from 0.1 to 1 AU, using $V = 1 \times 10^{-2}$ AU hr^{-1} and $V_{A0} = 1 \times 10^{-3}$ AU hr^{-1}. For $\delta = -3/2$ (Kraichnan spectrum), λ is roughly $\propto (V + V_A)^{5/2}$, decreasing by a factor of ≈ 4 when r is increased from 0.1 to 1 AU, and remaining almost constant as r is further increased. For $\delta = -4/3$, λ decreases to a minimum near $r = 0.6$ AU, and then rises slowly as r increases. Various r-dependences of λ based on SEP observations have been reported in the literature. For example, using the convection-diffusion model with the effective radial mean free path $\lambda_r \propto r^b$, Beeck et al. (1987) obtained $b = 0.5$ and $b = 0.7$ by fitting multispace-craft data to the 1977 December 27 and 1977 November 22 events, respectively. Zwickl & Webber (1977) and Hamilton (1977) found $b = 0$ and $b = 0.4$, respectively, by fitting SEP data measured on *Pioneer 10* and *11*. Feit (1973) found b from 0.8 to 1, while Webb et al. (1973) obtained negative values of b. Ng et al. (1983), using the focused transport model, found for a "scatter-free" event observed at 0.5 AU that $\lambda_\parallel$ decreased with r until $r \approx 0.5$ AU and then increased again further out. These studies are not necessarily in conflict, because they refer to different particle events, and more important, are based on observations at different values of r.

Including damping (i.e., $\gamma < 0$) in equation (27) causes I^h_+ to decrease faster and leads to a λ that decreases to a minimum and then increases with r further out. However, it suffices for our present purpose to adopt $\gamma = 0$ and $\delta = -3/2$ in equation (27). We then study the effect of the wave intensity level by varying I^h_{+0}, the reference differential wave intensity at the reference wavenumber k_0 and reference radius r_0.

2.2.6. *Numerical Solution*

To solve equation (14) numerically, we use time splitting and replace it by the following set of equations,

$$\frac{1}{2}\frac{\partial F}{\partial t}+\frac{\partial}{\partial r}(\mu v F)=0\,, \tag{31}$$

$$\frac{1}{2}\frac{\partial F}{\partial t}+\frac{\partial}{\partial \mu}\left(\frac{1-\mu^2}{r}vF\right)=\frac{\partial}{\partial \mu}\left(D_{\mu\mu}\frac{\partial F}{\partial \mu}\right)\,. \tag{32}$$

We define the grid $(\ln P_l,\ \mu_i,\ r_j,\ t_n)$, where $\ln P_l = \ln 16 + (l-1)\Delta(\ln P)$, $l = 1(1)L$; $\mu_i = (i+\frac{1}{2})\Delta\mu$, $i = -I(1)I-1$; $r_j = 0.1 + (j-1)\Delta r, j = 1(1)J$; $t_n = n\Delta t_0$, $n = 0, 1, \ldots$; and L, $2I$, and J denote the corresponding number of grid points. In most of the calculations, we use $L = 23$, $\Delta(\ln P) = (\ln 2)/8$ (P in MV), $I = 20$, $\Delta\mu = 1/I$, $J = 201$, $\Delta r = 0.0125$ AU, and $\Delta t_0 = 0.025$ hr. With F^n_{lij} replacing $F(P_l,\ \mu_i,\ r_j,\ t_n)$ and $D^n_{l,i+1/2,j}$ replacing $D_{\mu\mu}(P_l,\ \mu_i+\frac{1}{2}\Delta\mu,\ r_j,\ t_n)$, equations (31) and (32) are approximated by the following finite-difference equations, each with half time step $(\Delta t)/2$:

$$\left.\begin{aligned}\frac{F^{n+1/2}_{ij}-F^n_{ij}}{\Delta t}+\mu_i v_l\frac{\Delta_j F^n_{i,j-1}}{\Delta r}=0\,,\quad(\mu_i>0)\,,\\ \frac{F^{n+1/2}_{ij}-F^n_{ij}}{\Delta t}+\mu_i v_l\frac{\Delta_j F^n_{i,j}}{\Delta r}=0\,,\quad(\mu_i<0)\,,\end{aligned}\right\}, \tag{33}$$

$j = 1(1)J$, followed by antidiffusion flux correction (Book, Boris, & Hain 1975; Ng & Wong 1979; Wong 1982); and

$$\frac{F^{n+1}_{ij}-F^{n+1/2}_{ij}}{\Delta t}=-\frac{v_l}{r_j\Delta\mu}\Delta_i[(1-\mu^2_{i-1/2})F^{n+1/2}_{i-1,j}]+\frac{1}{(\Delta\mu)^2}\Delta_i(D^n_{i-1/2,j}\Delta_i F^{n+1}_{i-1,j})\,, \tag{34}$$

$i = -I(1)I-1$, also followed by antidiffusion flux correction. In the above, Δ_i and Δ_j denote forward difference with respect to the i and j indices, respectively. Note that $1-\mu^2_{i-1/2}$ and $D^n_{i-1/2,j}$ both vanish at $i = \pm I$. Since P_l (or v_l) appears only as a parameter in the above equations, the subscript l has been suppressed for convenience.

Equations (33) and (34) are conservative, and with antidiffusion flux correction, the effective truncation error should be better than the nominal truncation errors of $O(\Delta r)+O(\Delta t)$ and $O(\Delta\mu)+O(\Delta t)$, respectively. Equation (33) is solved explicitly for $F^{n+1/2}_{ij}$, sweeping in the j-direction for each value of i. Using $F^{n+1/2}_{ij}$, the implicit equation (34) is solved for F^{n+1}_{ij} by the Thomas algorithm, sweeping in the i-direction for each value of j. In each case the numerical diffusion error is reduced by antidiffusion flux correction. To ensure numerical stability and to keep the calculations for different rigidities in step, we choose the time step as follows (taking advantage of the nonrelativistic approximation): $\Delta t = \Delta t_0$, for $L = 1(1)8$; $\Delta t = (\Delta t_0)/2$, $L = 9(1)16$; $\Delta t = (\Delta t_0)/4$, $L = 17(1)23$.

The modulus of the local amplification factor of the finite-difference equations (33) and (34) is less than 1 if

$$\Delta t \le |\Delta r/(\mu_i v_l)|_{\min}\,, \tag{35}$$

$$\Delta t \le \left[\frac{r_j\Delta\mu}{(1-\mu^2_{i-1/2})v_l}+\frac{r_j^2(D^n_{l,i-1/2,j}+D^n_{l,i+1/2,j})}{(1-\mu^2_{i-1/2})^2 v_l^2}\right]_{\min}\,, \tag{36}$$

respectively, where "min" denotes the minimum value over the ij-grid. The combined stability requirement is the more stringent of the two.

The wave evolution equation (17) is approximated on the grid $(\log_{10}\eta_m,\ r_j,\ t_n)$, where $\log_{10}\eta_m = -2.0125 + (m-1)\Delta(\log_{10}\eta)$, $m = 1(1)M$. In most of the calculations, we use $\Delta(\log_{10}\eta) = 0.05$ and $M = 32$. The equation is solved by advancing from t_n to t_{n+1} assuming constant γ^h_d, i.e.,

$$I^h_d(\eta_m,\ r_j,\ t_{n+1}) = I^h_d(\eta_m,\ r_j,\ t_n)\exp(\gamma^h_d\Delta t_0)\,. \tag{37}$$

In the evaluation of $D_{\mu\mu}$ in equation (16), if $\log_{10}(\eta_L) - \frac{1}{2}\Delta(\log_{10}\eta) \le \log_{10}\eta_{\rm res} \le \log_{10}(\eta_U) + \frac{1}{2}\Delta(\log_{10}\eta)$, linear interpolation of I^h_d in $\log_{10}\eta$ is used; otherwise $D_{\mu\mu}$ is set to zero (subsequent modification renders it nonzero). Similarly, in the evaluation of γ^h_d in equation (18), if $P_L \le P_{\rm res} \le P_U$, linear interpolation of the integrand in $\ln P$ is made; if $P_{\rm res} > P_U$, extrapolation assuming, e.g., a P^δ spectrum is made, with e.g., $\delta = -8$; otherwise the integrand is set to zero. The integral is then evaluated numerically.

The cycle of calculation advancing F and I^h_d by one time step Δt_0 is as follows. I^h_d is used to calculate $D_{\mu\mu}$, which is used in advancing F by one time step; the new F is used to calculate γ^h_d, which is used to advance I^h_d. The cycle of calculation is then repeated as many times as desired.

The above grids have been chosen as a compromise between accuracy and reasonable running time and storage. In a number of test runs, we have confirmed that the calculated results do not differ significantly from those obtained using finer grids and smaller time steps.

3. RESULTS

3.1. *Attenuation of Differential Particle Intensity*

The contrast between the predictions obtained ignoring and including the effects of the streaming protons on the Alfvén waves is illustrated in Figure 1. In this figure we display the calculated time histories of the differential intensity $j_{\mathcal{E}}$, the anisotropy ξ, and the local mean free path λ of ~1 MeV protons at $r = 1.125$ AU, with and without taking into account the effect of particles on waves, all other parameters being identical. The proton source at $r = 0.1$ AU is set by $t_{\rm inj} = 1$ hr, $M(\mu) = \mu H(\mu)$, $j^0_{\mathcal{E}} = 2\times10^6$ (cm^2 s sr MeV)$^{-1}$, $P_0 = 43.33$ MV, $P_1 = 25$ MV and $P_2 = 21.6$ MV. The initial differential magnetic fluctuation intensities of the Alfvén waves are set via equation (27) by $I^{\rm L}_{+0} = I^{\rm R}_{+0} = I_0 = 1\times10^3$ MeV cm^{-2}, $I^{\rm L}_- = I^{\rm R}_- = 0.1I^{\rm R}_+$, $k_0/B_0 = 1/(43.33$ MV), $\delta = -1.5$, $\gamma = 0$, $V = 0.01$ AU hr^{-1}, and $V_{A0} = 1\times10^{-3}$ AU hr^{-1}. These give, for 1 MeV protons, $\lambda = 0.48$ AU at $r = 1$ AU increasing slowly to $\lambda = 1.1$ AU at $r = 0.2$ AU and more rapidly to $\lambda = 1.8$ AU near the inner boundary. The other parameters used in the run are $\Delta r = 0.0125$ AU, $\Delta\mu = 0.05$, $\Delta t_0 = 0.025$ hr, $\Delta(\ln P) = 0.08664$, and $\Delta(\log_{10}\eta) = 0.05$.

Figure 1 demonstrates that when the influence of the streaming protons on the Alfvén waves is taken into account, $j^{\rm max}_{\mathcal{E}}$, the maximum value of $j_{\mathcal{E}}$, is decreased by a factor ≈5 for 1 MeV protons at $r = 1.125$ AU, while the time of maximum $t_{\rm max}$ is increased from 4.9 hr to 5.7 hr. At $t \approx 1.6$ hr, before the arrival of the 1 MeV protons, λ starts to decrease from its initial value of 0.47 AU. This is due to the amplification of the local outward traveling right-hand polarized wave by *faster* protons that begin to arrive at this time. At $t = t_{\rm max} = 5.7$ hr, the decrease in λ at $r = 1.125$ AU from its initial value is only ~30%. The reason for the dramatic decrease in $j_{\mathcal{E}}$ is the much stronger wave growth at smaller values of r (see below).

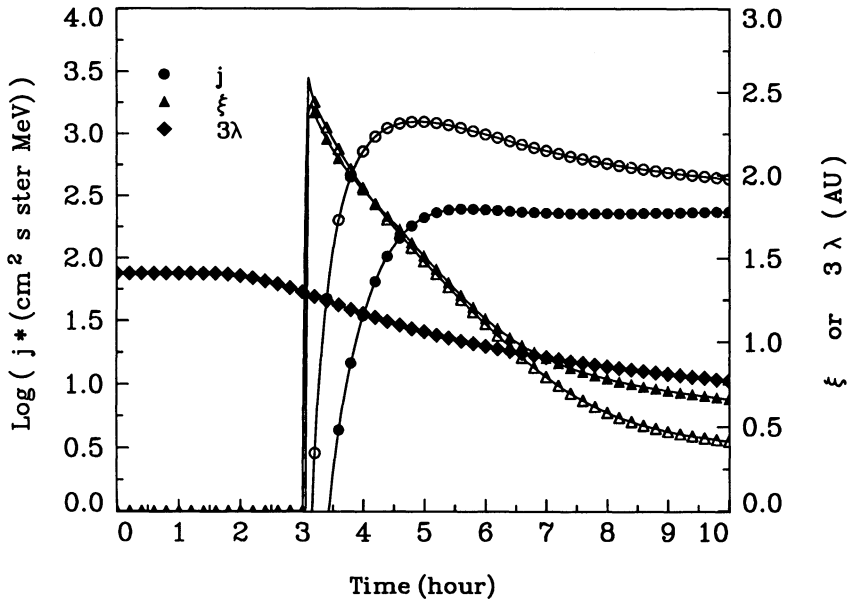

FIG. 1.—Time histories of the differential intensity $j_{\mathscr{E}}$, anisotropy ξ, and mean free path λ of 45 MV protons at $r = 1.125$ AU. Curves labeled with closed (*open*) symbols refer to the cases with (without) wave amplification/decay. $j^0_{\mathscr{E}} = 2 \times 10^6$ (cm^2 s sr MeV)$^{-1}$, $t_{\rm inj} = 1$ hr, and $I_0 = 1 \times 10^3$ MeV cm^{-2}. See text for other parameters.

Figures 2 and 3 display, at $r = 0.525$ AU and $r = 0.325$ AU, respectively, the time histories of the same quantities as depicted in Figure 1. The decrease of λ with t is now very significant, showing that wave growth is stronger at smaller r. The attenuation of $j^{\rm max}_{\mathscr{E}}$ decreases with decreasing r, since the "coherent pulse" has less time to "disperse" (Earl 1989). On the other hand, the amplified interplanetary Alfvén waves contribute to the extended "diffusive wake" in the intensity profile at the smaller values of r.

We have repeated the above calculations for a range of values of the source strength $j^0_{\mathscr{E}}$, *keeping all other parameters constant*. The results for 45 MV protons are summarized in Table 2, in which we list $j^{\rm max}_{\mathscr{E}}$ calculated with wave amplification, the ratio of $j^{\rm max}_{\mathscr{E}}$ and the ratio of $t_{\rm max}$, calculated with and without wave amplification, at $r = 0.325$, 0.525, and 1.125 AU, respectively, for proton source strength $j^0_{\mathscr{E}}$ ranging from 1.25×10^5 (cm^2 s sr MeV)$^{-1}$ to 4×10^6 (cm^2 s sr MeV)$^{-1}$. We also find that as $j^0_{\mathscr{E}}$ is decreased, the calculated $j_{\mathscr{E}}$ versus t and ξ versus t curves at $r = 1.125$ AU for the cases with and without wave amplification merge, becoming almost indistinguishable when $j^0_{\mathscr{E}} \lesssim 5 \times 10^4$ (cm^2 s sr MeV)$^{-1}$, or alternatively, when $j^{\rm max}_{\mathscr{E}} \lesssim 30$ (cm^2 s sr MeV)$^{-1}$ at $r = 1.125$ AU. From Table 2, we see that $j^{\rm max}_{\mathscr{E}}$ at 1.125 AU is significantly attenuated by wave amplification when $j^0_{\mathscr{E}} > 5 \times 10^5$ (cm^2 s sr MeV)$^{-1}$, or to put it another way, when $j^{\rm max}_{\mathscr{E}}$ at $r = 1.125$ AU calculated with wave amplification exceeds $\approx 2 \times 10^2$ (cm^2 s sr MeV)$^{-1}$. An inter-

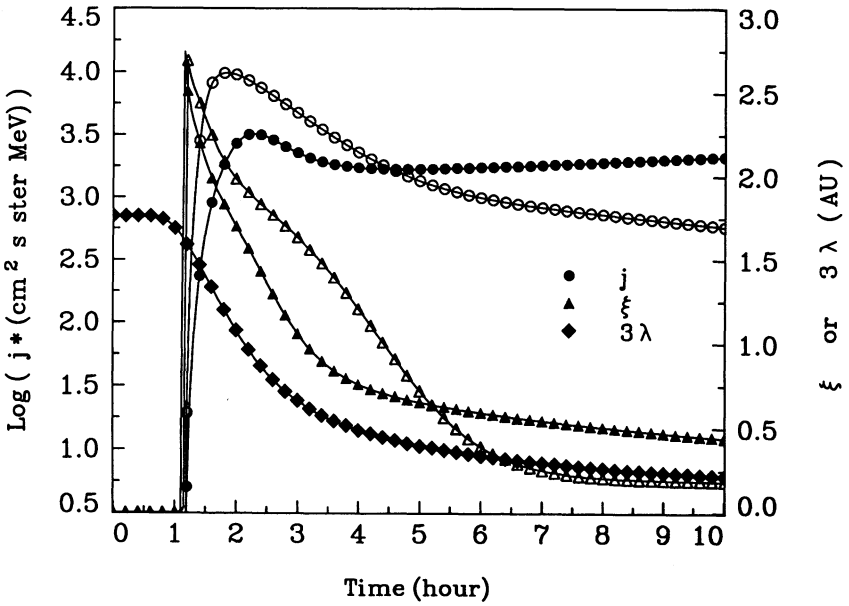

FIG. 2.—Same as Fig. 1, but at $r = 0.525$ AU

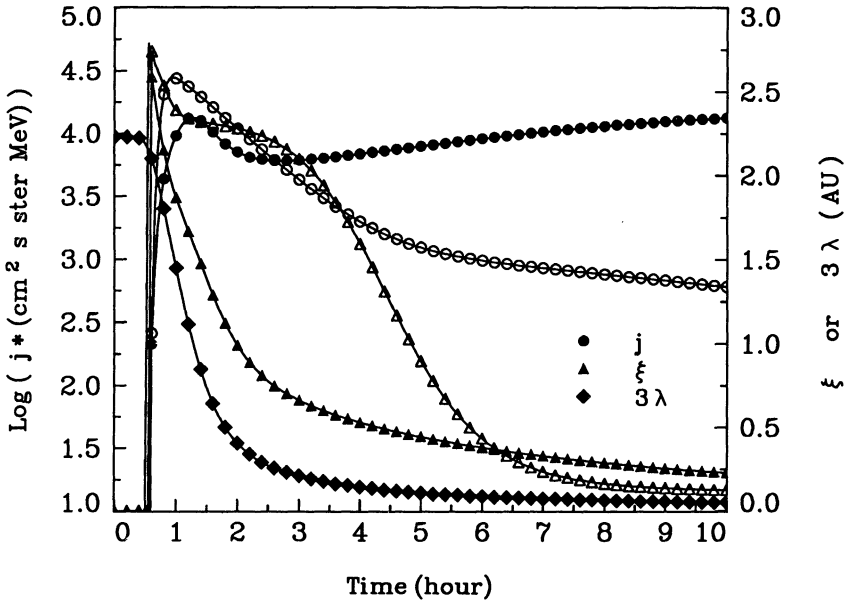

FIG. 3.—Same as Fig. 1, but at $r = 0.325$ AU

esting feature here is that, as the source strength $j_{\mathscr{E}}^0$ is increased $j_{\mathscr{E}}^{\max}$ at $r = 1.125$ AU peaks at $\approx 2.5 \times 10^2$ (cm^2 s sr MeV)$^{-1}$.

From Table 2 we also see that at $r = 1.125$ AU the increase in $t_{\max}$ due to wave amplificiation is $\lesssim 18\%$. If we regard the lower $j_{\mathscr{E}}$ curve in Figure 1 as the "observation," and attempt to fit it using the focused transport model with the same injection time profile but ignoring wave amplification, we may underestimate λ by $\sim 18\%$ and $j_{\mathscr{E}}^0$ by a factor of 5. Furthermore, because $j_{\mathscr{E}}^{\max}$ decreases as $j_{\mathscr{E}}^0$ at $r = 1.125$ AU is increased beyond $\approx 1 \times 10^6$ (cm^2 s sr MeV)$^{-1}$, we may underestimate the source strength by an even larger factor. Note that the classical radial diffusion model with a mean free path independent of r and t would produce the same $t_{\max}$ with an even smaller λ of ≈ 0.34 AU. However, it is not really meaningful, where wave growth is important, to refer to λ as a constant or as a function of r alone, since it is strongly dependent on both r and t (see Fig. 6 below).

We may try to understand the dependence of $j_{\mathscr{E}}^{\max}$ and $t_{\max}$ on $j_{\mathscr{E}}^0$ in the wave-particle coupled model with time-dependent λ by examining how $j_{\mathscr{E}}^{\max}$ and $t_{\max}$ depend on the spatial dependence of the time-independent λ in the classical diffusion model, for which analytical solution is available. Let us consider the spherically symmetric radial diffusion model, with an impulsive δ-function source at $r = 0$ and a radial mean free path $\lambda_r = \lambda_0(r/1\ \mathrm{AU})^{\beta}$, λ_0 and β being constants. The solution is

$$j_{\mathscr{E}}(r, t) = \frac{N}{4\pi\Gamma(\epsilon)} \left(\frac{\epsilon}{3}\right)^{2\epsilon-1} \left(\frac{3}{\lambda_0 vt}\right)^{\epsilon} \exp\left[-\frac{3r^{2-\beta}}{(2-\beta)^2\lambda_0 vt}\right], \quad (38)$$

where $\epsilon = 3/(2-\beta)$, and N is a constant related to the source strength (Parker 1963). It gives

$$t_{\max} = r^{2-\beta}/[(2-\beta)v\lambda_0], \quad (39)$$

$$j_{\mathscr{E}}^{\max}(r) = \frac{N}{4\pi r^3} \frac{3e^{-\epsilon}\epsilon^{\epsilon-1}}{\Gamma(\epsilon)}. \quad (40)$$

Using Stirling's formula for gamma function, we may show that

$$j_{\mathscr{E}}^{\max}(r) \sim \frac{N}{4\pi r^3}\left[\frac{3(2-\beta)}{2\pi}\right]^{1/2} \to 0 \quad \text{as } \beta \to 2-. \quad (41)$$

Note that in equation (40), $4\pi r^3 j_{\mathscr{E}}^{\max}(r)/N$ is independent of λ_0, being equal to 0.925 for $\beta = 0$, and 0.2179 for $\beta = 1.9$, and vanishing as $\beta \to 2-$. This may be understood as a result of the

TABLE 2

$j_{\mathscr{E}}^{\max}$, $j_{\mathscr{E}}^{\max}$ RATIO AND $t_{\max}$ RATIO OF 45 MV PROTONS[a]

r	0.33	0.53	1.13	0.33	0.53	1.13	0.33	0.53	1.13
($j_{\mathscr{E}}^0/10^5$)	($j_{\mathscr{E}}^{\max}/10^3$)	($j_{\mathscr{E}}^{\max}/10^3$)	($j_{\mathscr{E}}^{\max}/10^2$)	$j_{\mathscr{E}}^{\max}$ Ratio[b]			$t_{\max}$ Ratio[b]		
1.3	1.57	0.51	0.67	0.89	0.83	0.86	1.01	1.04	1.07
2.5	2.76	0.91	1.22	0.79	0.74	0.78	1.02	1.18	1.13
5.0	5.21	1.66	2.01	0.74	0.68	0.64	1.51	1.31	1.18
10	9.33	2.61	2.54	0.67	0.53	0.41	1.44	1.28	1.17
20	13.4	3.21	2.46	0.48	0.33	0.20	1.33	1.23	1.16
40	15.1	3.08	1.94	0.27	0.16	0.08	1.28	1.22	1.18

[a] Model parameters are as for Fig. 1; r is in AU; $j_{\mathscr{E}}^0$ and $j_{\mathscr{E}}^{\max}$ are in (cm^2 s sr MeV)$^{-1}$.

[b] These ratios refer to the value calculated with wave growth divided by the value calculated without wave growth.

particles spending more time dispersing over a larger volume, thus reducing the maximum intensity at any given r.

If we regard the time-dependent model as being characterized by an effective β that increases with time because of the r-dependent wave amplification, then since the effective value of β clearly increases with $j_\mathcal{E}^0$, we expect the $j_\mathcal{E}^{max}$ ratio to decrease and the t_{max} ratio to increase as $j_\mathcal{E}^0$ is increased, in analogy with the classicial diffusion model (eqs [41] and [39]). The former but not the latter behavior is in qualitative accord with Table 2. Quite apart from the difficulty of comparing the linear diffusion model with the nonlinear coupled model, we note the following limitations in the above analogy: (1) where $\lambda \gtrsim r$, the diffusion model should be replaced by the focused transport model which would give t_{max} weakly dependent on λ, and (2) the growing waves clearly have more influence over particles that arrive later than particles that arrive earlier. In view of point (1) above, we expect t_{max} to be more greatly increased by wave growth as I_0 is increased. This is indeed the case. The effects of initial wave spectrum will be discussed later.

The time histories of the 1 MeV proton pitch distribution and $D_{\mu\mu}/v$ at $r = 0.325$ AU are shown in Figures 4 and 5, respectively. The former shows the arrival of the anisotropic coherent pulse, followed by an extensive diffusive wake (Earl 1976). The latter shows the effect of Alfvén wave evolution driven by particle anisotropy at all rigidities. Figure 6 shows that the mean free path of 45 MV protons evolves rapidly from an initially decreasing function of r to an increasing function of r, because of the r-dependent growth of outward travelling Alfvén waves. After $\partial f/\partial\mu$ has decreased to a small value, the $\partial f/\partial P$ term may dominate equation (11), leading to damping of I_+^L and I_+^R. However, this is only significant at $r < 0.15$ AU. For example, at $r = 0.125$ AU, λ decreases rapidly from 1.7 AU at $t = 0$ to 0.004 AU at $t = 1.2h$, and then increases steadily, exceeding 7 AU at $t > 7$ hr. However, because wave propagation and momentum transport are neglected, this later increase of λ at $r < 0.15$ AU should not be taken seriously.

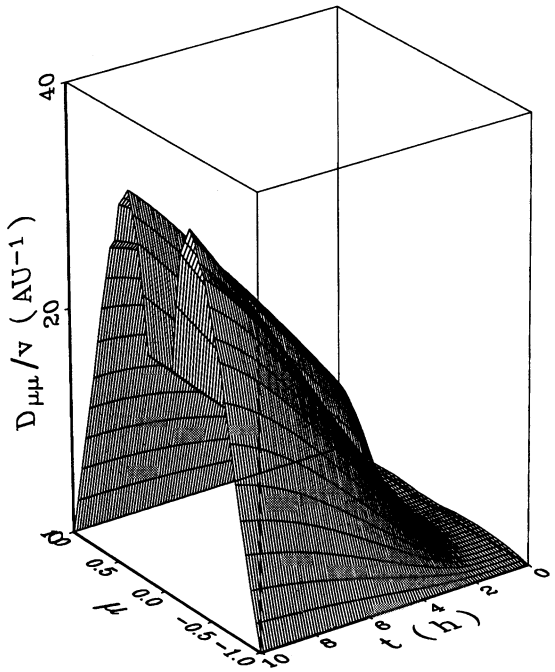

FIG. 5.—The pitch diffusion coefficient of 45 MV protons at $r = 0.325$ AU as a function of μ and t. Parameters are as for Fig. 1.

3.2. *Evolution of Interplanetary Alfvén Waves*

Let us now examine the differential intensities of magnetic field fluctuation of the Alfvén waves. For the same parameters

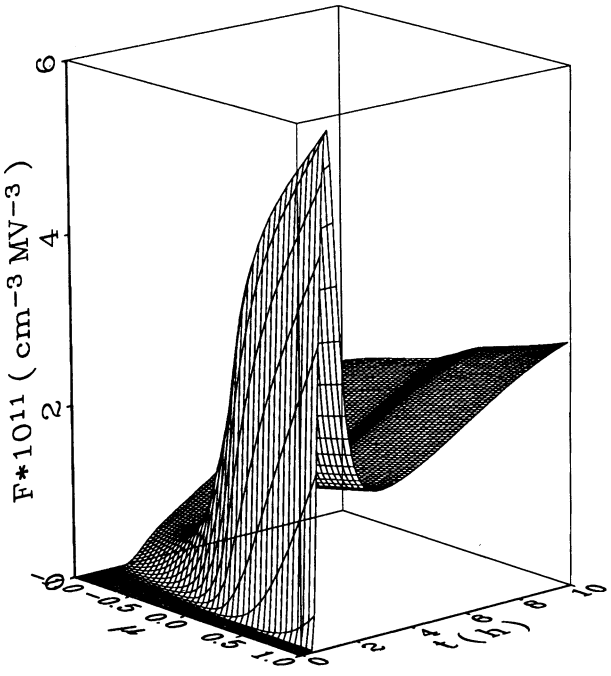

FIG. 4.—The evolution of the pitch distribution of 45 MV protons at $r = 0.325$ AU, showing the arrival of the coherent pulse and the development of the diffusive wake. The model parameters are as for Fig. 1. Note the linear vertical scale.

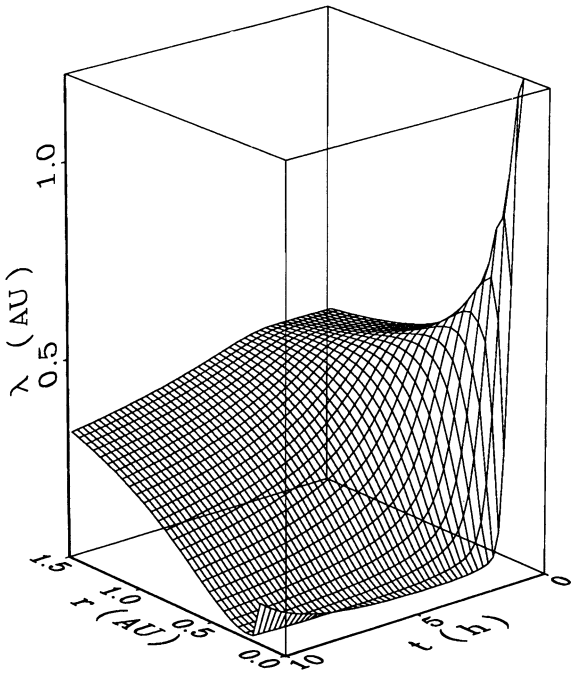

FIG. 6.—The mean free path of 45 MV protons as a function of r and t. Parameters are as for Fig. 1.

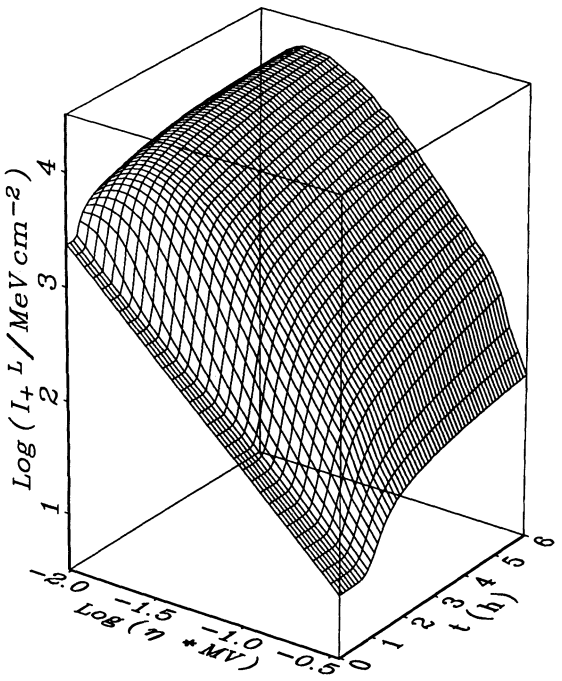

FIG. 7.—The evolution of the differential magnetic fluctuation intensity I_+^L of the outward right-hand polarized Alfvén wave at $r = 0.325$ AU. Parameters are as for Fig. 1.

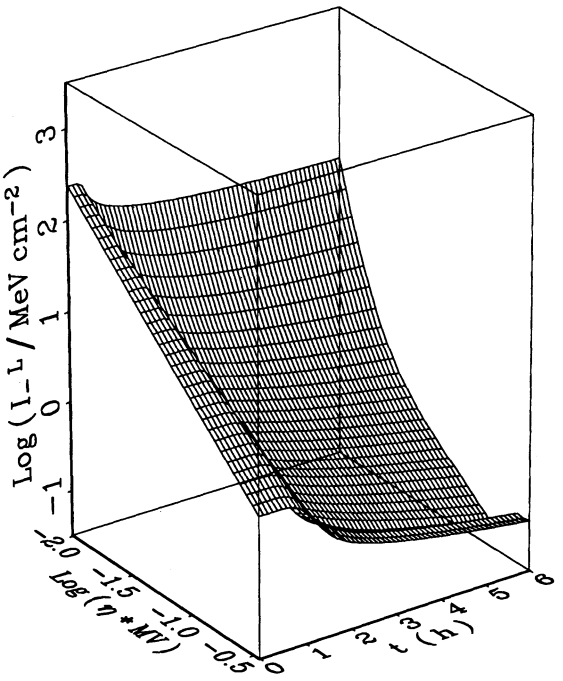

FIG. 9.—Same as Fig. 7, but for inward right-hand polarized Alfvén waves I_-^L.

as in Figure 1, Figures 7, 8, 9, and 10 show, respectively, the evolution of I_+^L, I_+^R, I_-^L and I_-^R at $r = 0.325$ AU. We have assumed here that $B > 0$; if $B < 0$, we should change the helicity labels in these figures (the polarizations remain the same). Figure 7 shows I_+^L increases by an order of magnitude in ~ 2 hr. Faster protons arrive earlier to amplify the waves at lower wavenumbers. Figure 9 shows the simultaneous decay in I_-^L. Figure 8 shows the later and slower rise of I_+^R (relative to I_+^L), which is due to protons that have diffused to $\mu < (V + V_A)/v - 1/(P\eta_U)$. In a solar particle event, we have mostly $\partial f/\partial\mu > 0$ for all values of μ. Simultaneously I_-^R decays as depicted in Figure 10.

Taken together, the overall effect of the particle-driven wave evolution is to increase $D_{\mu\mu}$ and decrease λ. The damping of the

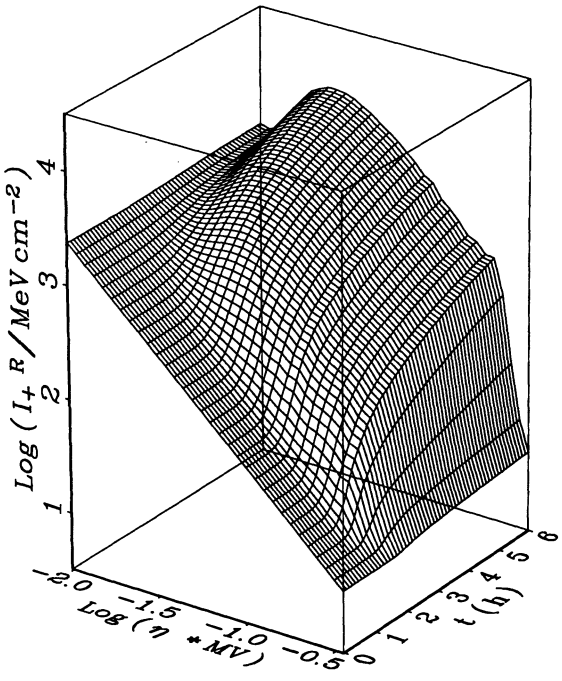

FIG. 8.—Same as Fig. 7, but for outward left-hand polarized Alfvén waves I_+^R.

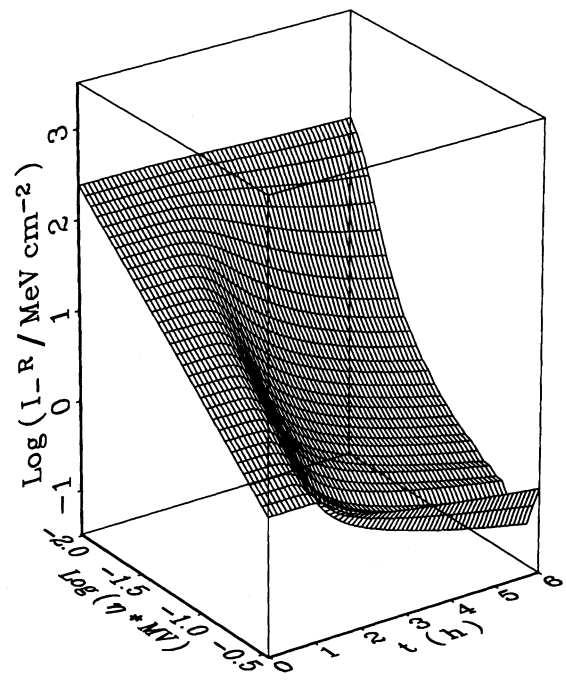

FIG. 10.—Same as Fig. 7, but for inward left-hand polarized Alfvén waves I_-^R.

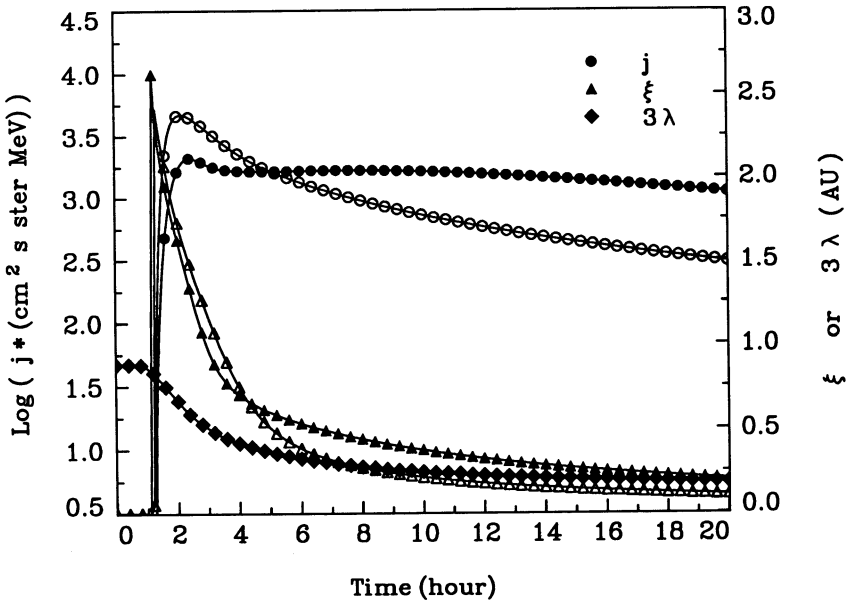

FIG. 11.—Showing the effect of doubling I_0 and halving j_g^0. Same as Fig. 2 ($r = 0.525$ AU), except $j_g^0 = 1 \times 10^6$ (cm^2 s sr MeV)$^{-1}$, and $I_0 = 2 \times 10^3$ MeV cm^{-2}

inward propagating waves is completely outweighed by the growth of the inward traveling waves; this is true even if we start with equal intensities of outward and inward propagating waves.

Finally, we examine a point of consistency here. The wave dispersion relation (8) and wave growth rate (11) apply under the assumption that $\gamma_d^h \ll \omega$. For the calculation presented above, the momentarily attained maximum value of $|\gamma_d^h/\omega|$ is 0.018, for I_+^R at $\eta = 3.868 \times 10^{-2}$ MV^{-1}, $r = 0.1125$ AU and $t = 0.275$ hr.

3.3. *Initial Wave Spectrum*

Figures 11 and 12 show, at $r = 0.525$ AU and $r = 1.125$ AU, respectively, the various time histories as in Figures 2 and 1, all parameters being identicial to those for Figures 2 and 1 except that the initial wave intensity level has been doubled: $I_0 = 2 \times 10^3$ MeV cm^{-2}, and the proton source strength halved: $j_g^0 = 1 \times 10^6$ (cm^2 s sr MeV)$^{-1}$. Figure 11 shows that at $r = 0.525$ AU, the j_g^{max} ratio and t_{max} ratio between the cases with/without wave evolution are 0.45 and 1.14, respectively. These ratios are not very different from those (0.53 and 1.28, respectively) given in Table 2 for half the wave intensity level: $I_0 = 1 \times 10^3$ MeV cm^{-2} and the same proton source strength. In contrast, Figure 12 shows that at $r = 1.125$ AU, j_g peaks at $t_{max} = 19.2$ hr, the t_{max} ratio is 3.04, and the j_g^{max} ratio is 0.57, compared with 5.75 hr, 1.17, and 0.41, respectively when $I_0 = 1 \times 10^3$ MeV cm^{-2} (Table 2).

Why does doubling the initial wave intensity level from

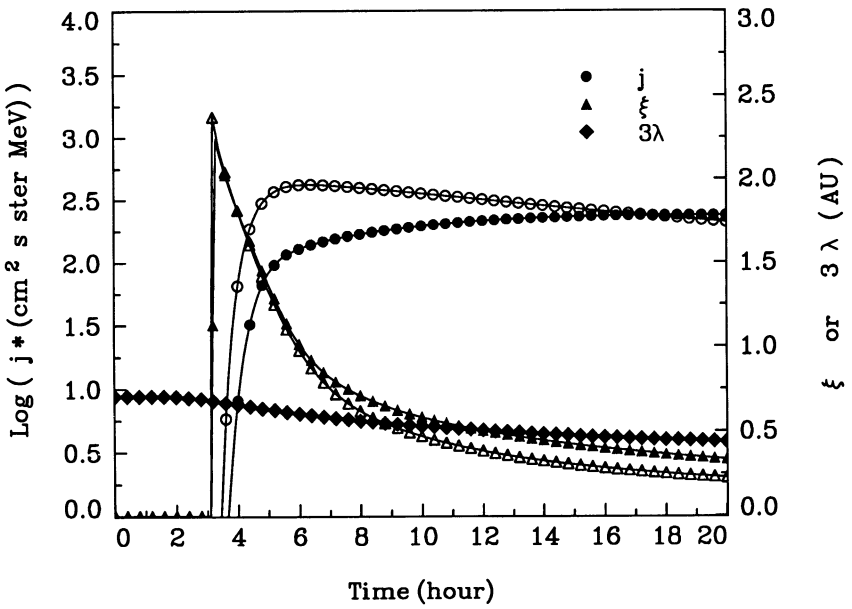

FIG. 12.—Same as Fig. 11, except $r = 1.125$ AU

$I_0 = 1 \times 10^3$ MeV cm^{-2} to $I_0 = 2 \times 10^3$ MeV cm^{-2} produce such a significant change in t_{max} at $r = 1.125$ AU and not at 0.525 AU? The answer lies in the transition from supercoherent and coherent transport to diffusive transport as r increases (Earl 1976). Particle transport is supercoherent where $|(\lambda/B)\partial B/\partial r| = 2\lambda/r \gg 1$, coherent where $\lambda \sim r$, and diffusive where $\lambda \ll r$. In the supercoherent and coherent regimes, t_{max} is not very sensitive to λ; whereas in the diffusive regime (see eq. [39]), $t_{max} \propto 1/\lambda$, or equivalently, $t_{max} \propto I_0$. For $I_0 = 2 \times 10^3$ MeV cm^{-2}, at $t = 0$ hr, we have $\lambda = 0.235$ AU at $r = 1.125$ AU, increasing to $\lambda = 0.55$ AU at $r = 0.2$ AU, and $\lambda = 0.9$ AU near the inner boundary. This means that initially $r = 1.125$ AU is just inside or just outside the diffusive regime, whereas $r = 0.525$ AU is in the coherent regime. The reduction in λ due to wave growth therefore produces a significant reduction in t_{max} at $r = 1.125$ AU but not at $r = 0.525$ AU. For $I_0 = 1 \times 10^3$ MeV cm^{-2}, however, $r = 1.125$ AU lies also in the coherent regime, so that t_{max} there does not respond sensitively to wave growth.

Thus, paradoxical as it might appear, even though wave growth decreases with increasing r, its effect on the proton intensity time profile is greater at larger values of r. One may expect that as I_0 is further increased, the strong diffusive dependence of t_{max} on λ and hence on I_0 will extend further inward to smaller values of r. Figure 13 shows the various time histories at $r = 0.325$ AU for $I_0 = 2 \times 10^4$ MeV cm^{-2}, and all other parameters as for Figures 1–3. The initial λ is 20 times smaller than in Figure 3, so that even at this small distance $r = 0.325$ AU, when wave evolution is turned on, t_{max} is increased from 3.8 to 15.6 hr. However, $j_{\mathcal{E}}^{max}$ hardly suffers any change in this case.

3.4. *Pitch Dependence of the Proton Source*

Changing the μ-dependence of the particle source from $\mathcal{M}(\mu) = \mu H(\mu)$ to $\mathcal{M}(\mu) = H(\mu)$ while keeping $j_{\mathcal{E}}^0$ constant doubles the flux of source particles. On the one hand, the smaller $\partial f/\partial \mu$ near the source location gives slower wave growth there; on the other hand, focusing leads to larger $\partial f/\partial \mu$ and faster wave growth further out. In the absence of wave growth, for $j_{\mathcal{E}}^0 = 2 \times 10^6$ (cm^2 s sr MeV)$^{-1}$, $j_{\mathcal{E}}^{max}$ at $r \gtrsim 0.3$ AU calculated with $\mathcal{M}(\mu) = H(\mu)$ is only ≈ 1.5 times $j_{\mathcal{E}}^{max}$ calculated with $\mathcal{M}(\mu) = \mu H(\mu)$. In the presence of wave growth, however, the calculated $j_{\mathcal{E}}^{max}$ for $\mathcal{M}(\mu) = H(\mu)$ is 1.50×10^4, 3.25×10^3, and 2.19×10^2 (cm^2 s sr MeV)$^{-1}$ at $r = 0.325$, 0.525, and 1.125 AU respectively, while the corresponding values for $\mathcal{M}(\mu) = \mu H(\mu)$ are not significantly different, viz., 1.34×10^4, 3.21×10^3, and 2.46×10^2 (cm^2 s sr MeV)$^{-1}$. Apparently, for both forms of $\mathcal{M}(\mu)$ the particles that arrive at $t = t_{max}$ at $r \gtrsim 0.3$ AU are mainly those initially injected at μ close to 1.

3.5. *Resonance Gap*

In the sections above, we have adopted the average of the two values of $D_{\mu\mu}$ just outside the approximate "resonance gap" $(V + V_A)/v - 1/(P\eta_U) < \mu < (V + V_A)/v + 1/(P\eta_U)$, as the values of $D_{\mu\mu}$ inside the gap. This is a heuristic procedure to take account of the finite scattering of protons with pitch angles inside the gap, as a realistic treatment including other wave modes and nonlinear resonance broadening is outside the scope of this paper. It is thus desirable to get an idea of the extent to which the results depend on the above assumption, by varying the procedure of filling the $D_{\mu\mu}$ values in the gap.

Filling in the gap by using α times the above average, with $\alpha = 0.5$ and all other parameters identical to those for Figure 1, raises somewhat the $j_{\mathcal{E}}$ versus t profile of 1 MeV proton at $r = 1.125$ AU—the j_{max} ratio is now 0.27 and the t_{max} ratio is 1.14, to be compared with 0.20 and 1.16, respectively for Figure 1. However, the differential wave intensity I_+^L, at $r = 0.325$ AU for example, grows to an order of magnitude larger at the highest frequencies $\eta > 0.24$ MV^{-1}, as compared to Figure 4. Thus, a smaller effective $D_{\mu\mu}$ in the gap results in faster and larger wave growth at the highest frequencies, as $\partial f/\partial \mu$ becomes larger just outside the gap. Choosing $\alpha = 0.2$ causes the wave intensity to grow out of bound. We choose $\alpha = 1$ as above as it produces a relatively smooth wave spectrum.

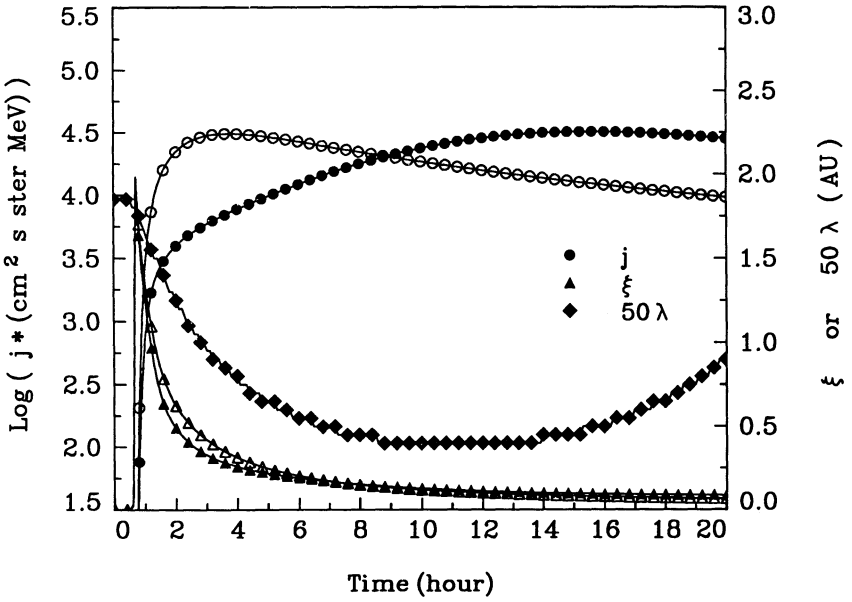

FIG. 13.—Showing the effect of 20 times larger initial wave intensities. Same as Fig. 3, except $I_0 = 2 \times 10^4$ MeV cm^{-2}. Note that λ is multiplied by 50.

3.6. *Alfvén Speed*

Equation (18) implies that the rates of wave growth and decay are approximately proportional to the Alfvén speed V_A. With all other parameters identical to those used for Figure 1, halving V_{A0} from 1×10^{-3} AU hr^{-1} to 5×10^{-4} AU hr^{-1} causes the $j_{\mathscr{E}}^{max}$ ratios at $r = 0.325$, 0.525, and 1.125 AU to increase from 0.48, 0.33, and 0.20 to 0.62, 0.49, and 0.37, respectively, while the t_{max} ratios remain essentially unchanged at 1.33, 1.23, and 1.26 respectively. If, in addition to halving V_{A0}, we also double $j_{\mathscr{E}}^0$ to 4×10^6 (cm^2 s sr MeV)$^{-1}$, then $j_{\mathscr{E}}^{max}$ ratios become 0.43, 0.28, 0.17, and the t_{max} ratios become 1.27, 1.19, and 1.16, respectively. The effects of doubling $j_{\mathscr{E}}^0$ and halving V_{A0} roughly compensate one another. Note, however, that halving V_{A0} also has the effect of introducing less spatial variation in λ (see eq. [27]).

3.7. *Extended Injection*

Figure 14 shows the time histories of $j_{\mathscr{E}}$, ξ, and λ from $t = 0$ to $t = 20$ hr at $r = 1.125$ AU, calculated with all parameters as for Figure 1 except $t_{inj} = 4$ hr (4 times larger) and $j_{\mathscr{E}}^0 = 5 \times 10^5$ (cm^2 s sr MeV)$^{-1}$ (4 times smaller). Note the plateau-like $j_{\mathscr{E}}$ versus t curve. The t_{max} value in the absence (presence) of wave evolution is 6.4 hr (6.1 hr), compared with 4.9 hr (5.7 hr) in Figure 1. The j_{max} ratio in Figure 14 is 0.38 compared to 0.20 in Figure 1. Figure 15 shows that the same calculations as for Figure 14 produces at $r = 0.325$ AU a prominent diffusive wake somewhat higher than the coherent pulse, the peak in the coherent pulse being depressed by 17% and delayed by 58% relative to the case without wave evolution. Comparison of Figure 1 with Figure 14 and Figure 3 with Figure 15 illustrates that increasing t_{inj} and decreasing $j_{\mathscr{E}}^0$ while keeping $j_{\mathscr{E}}^0 t_{inj}$ constant leads to a more prominent diffusive wake and to less attenuation of the coherent pulse. Apart from the extended injection itself, the distribution of wave growth over a wider region probably also plays a significant role in producing the above features. However, the prediction at $t \gg t_{max}$ should not be taken seriously because of the neglect of wave propagation and particle momentum transport.

3.8. *Source Rigidity Spectrum*

Equation (11) shows that $\partial f/\partial\mu$ dominates the wave growth (decay) rates until the proton distribution approaches isotropy. Therefore the proton source strength parameter $j_{\mathscr{E}}^0$ determines the overall level of wave growth (decay), and the spectral shape of the proton source influences the relative levels of wave growth (decay) at different wavenumbers.

Changing the parameters $P1$ and $P2$ in equation (21) from $P1 = 25$ MV and $P2 = 21.6$ MV used above to $P1 = 50$ MV and $P2 = 20.61$ MV yields a harder source spectrum than before: the energy spectral index $\partial \log (P^2\mathscr{F})/\partial \log \mathscr{E}$ remains at 1 at 136 keV, decreases to 0 at 300 keV, -0.71 at 1 MeV, and -1.54 at 6 MeV. There are now more source protons at >1 MeV than before. With the new source spectrum, and extrapolation of F with a P^{-7} spectrum, and all other parameters as for Figure 1, the model yields, at $r = 0.325$ AU, I_+^L up to a factor of 3 larger at $\eta < 2 \times 10^{-2}$ MV^{-1}, and only ~20% larger at $\eta > 1.5 \times 10^{-1}$ MV^{-1}. Since higher energy protons travel ahead to amplify the outward waves which slower energy protons encounter later, a harder source spectrum should attenuate the differential intensity of 1 MeV protons more strongly. The model gives at $r = 0.325$, 0.525, and 1.125 AU, j_{max} ratio = 0.36, 0.19, and 0.087, respectively (compared with 0.48, 0.33, and 0.22 in Figs. 1, 2, and 3), and t_{max} ratio = 1.32, 1.25, and 1.26 respectively (compared with 1.33, 1.23, and 1.16 in Figs. 1, 2, and 3).

A peak or flattening in solar proton spectra is sometimes observed in the 100 keV region (Reames et al. 1992). Peaks are also produced in some theoretical spectra (see, e.g., Forman et al. 1986). So far the proton source spectra we used have a peak at 260 or 300 keV. Does wave growth depend on the presence of a spectral peak? To answer this question, we set $P_1 = 43.33$ MV and $P_2 = 0$ MV, obtaining a monotonic decreasing spec-

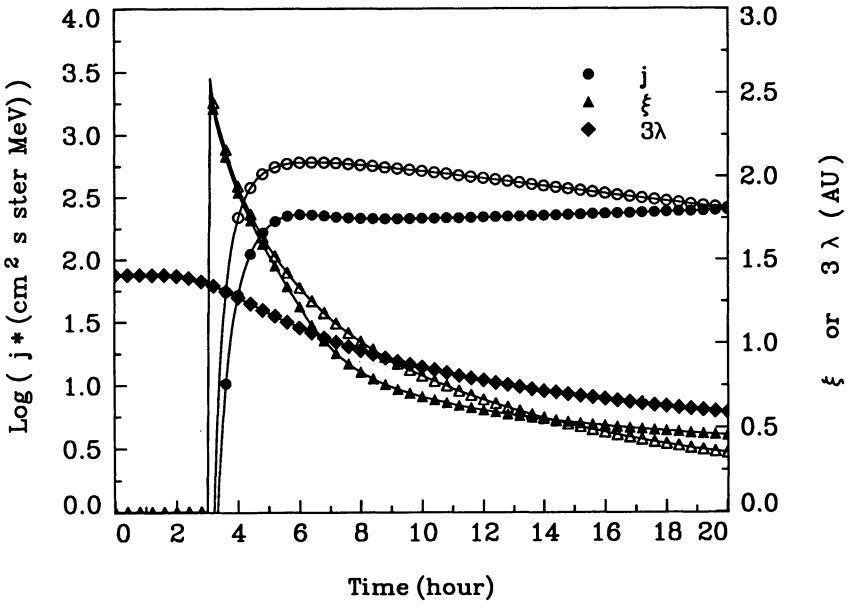

FIG. 14.—Showing the effect of increasing t_{inj} and decreasing $j_{\mathscr{E}}^0$ by a factor of 4. Same as Fig. 2 ($r = 0.525$ AU), except $j_{\mathscr{E}}^0 = 5 \times 10^5$ (cm^2 s sr MeV)$^{-1}$, and $t_{inj} = 4$ hr.

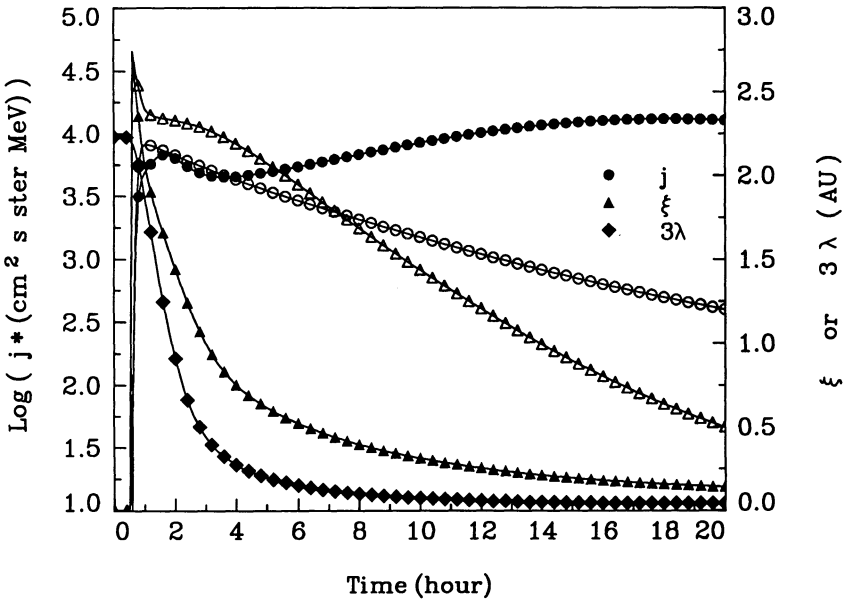

FIG. 15.—Same as Fig. 14, except $r = 0.325$ AU

trum in $P^2\mathscr{J}$, the energy spectral index of which steepens from -0.69 at 136 keV to -1 at 1 MeV and to -1.74 at 6 MeV. For this source spectrum, the model predicts I_+^L at $r = 0.325$ AU intermediate between the two previous cases, $j_{\max}$ ratio = 0.40, 0.24, and 0.12, $t_{\max}$ ratio = 1.32, 1.24, and 1.20 at $r = 0.325$, 0.525, and 1.125 AU, respectively. Thus, wave growth does not depend on the presence of a spectral peak in the proton source.

4. DISCUSSION

The main predictions of the model are summarized below.

1. For reasonable values of the model parameters, following the arrival of a sufficiently strong flux of SEP, the outward right-hand polarized Alfvén waves grow rapidly by roughly more than an order of magnitude at $r \lesssim 0.3$ AU, followed later by the left-hand polarized Alfvén waves, while the inward Alfvén waves decay. The growth or decay of the differential wave intensities decreases with increasing heliocentric distance r.

2. The influence of the particle-driven r-dependent wave growth on the proton differential intensity $j_{\mathscr{E}}$ at 1 MeV depends on the proton source strength parameter $j_{\mathscr{E}}^0$, the injection timescale $t_{\rm inj}$, the source spectrum, the initial wave differential intensity parameter I_0, the Alfvén speed parameter V_{A0}, and the observer's location r. With $V_{A0} = 1 \times 10^{-3}$ AU hr^{-1}, $I_0 = 1 \times 10^3$ MeV cm^{-2}, and $t_{\rm inj} = 1$ hr, the effect of wave evolution on $j_{\mathscr{E}}$ at $r \gtrsim 0.3$ AU is negligible for $j_{\mathscr{E}}^0 \lesssim 5 \times 10^4$ (cm^2 s sr MeV)$^{-1}$ or for $j_{\mathscr{E}}^{\max} \lesssim 30$ (cm^2 s sr MeV)$^{-1}$ at $r \approx 1$ AU. As $j_{\mathscr{E}}^0$ is increased, the maximum proton differential intensity $j_{\mathscr{E}}^{\max}$ at $r \approx 1$ AU rises to a peak of $\approx 2.5 \times 10^2$ (cm^2 s sr MeV)$^{-1}$ and then decreases slowly. The ratio of $j_{\mathscr{E}}^{\max}$ calculated with wave evolution to $j_{\mathscr{E}}^{\max}$ calculated without wave evolution is listed in Table 2 and decreases with r. The time-of-maximum $t_{\max}$ does not depend sensitively on $j_{\mathscr{E}}^0$ unless r and I_0 are large enough to place the observer in the (spatially) diffusive regime. Increasing V_{A0} or injecting a harder spectrum of protons causes the wave growth or damping to increase and $j_{\mathscr{E}}^{\max}$ to decrease.

The above predictions are in qualitative or semiquantitative agreement with the observations of SEP at $r \approx 1$ AU that indicate (1) small impulsive events have large mean free path $\lambda \gtrsim 0.5$ AU, whereas large gradual events tend to have smaller effective values of $\lambda \lesssim 0.1$ AU, and (2) $j_{\mathscr{E}}^{\max}$ seldom exceeds $\approx 5 \times 10^2$ (cm^2 s sr MeV)$^{-1}$ (Reames 1990, 1993). The model predicts that $j_{\mathscr{E}}^{\max}$ at $r \approx 1$ AU does not exceed $\approx 2.5 \times 10^2$ (cm^2 s sr MeV)$^{-1}$. In view of the simplified nature of the model, the prediction and observation may be regarded as in good agreement. The results of the model suggest that for large impulsive SEP events, the classical model underestimates significantly the particle source strength, and if the initial wave intensity is sufficiently high, gives a fitted mean free path significantly smaller than what initially characterizes the interplanetary space. Its prediction of the *r-dependent* growth of outward Alfvén waves is relevant to models of ion acceleration at a traveling interplanetary shock (e.g., Lee & Ryan 1986; Cane et al. 1988) as it implies that energetic ions traveling upstream would amplify interplanetary hydromagnetic waves sufficiently to make the shock an efficient accelerator. Of course the shock must be strong enough for the acceleration to override adiabatic deceleration, and r may have to exceed a minimum value for this to happen.

To make the model tractable, we have made a number of simplifying assumptions.

1. The model does not consider particle momentum transport, whereas clearly the particles must lose energy to amplify the waves. Momentum transport, however, proceeds slower than pitch diffusion by a factor of $O(V_A/v)$, which has a maximum value of $\approx 7 \times 10^{-2}$ for 16 MV protons at the smallest r. We note also the timescale of adiabatic deceleration $r/(2V)$ is ~ 5.6 hr at $r = 0.1125$ AU and 50 hr at $r = 0.3$ AU. Thus the neglect of momentum transport is justified for our purpose—it appears to invalidate the calculation only at some time after $t_{\max}$. On the other hand, if the protons are accelerated by a traveling forward interplanetary shock, then their energy loss to the upstream waves may be more than offset by, for example, their energy gain from the downstream waves.

2. Only amplification or damping of the Alfvén waves due to quasi-linear resonant interactions with SEP is considered in

the model. Nonlinear wave-wave interaction may cause the wave intensities to saturate or decay (see, e.g., Omura & Matsumoto 1989) and limit the size of the attenuation of proton intensity. This raises the possibility that for a large proton source the present model may overestimate the effect of self-amplified waves. This difficult issue probably can only be addressed through plasma simulation. For now, we show that wave amplification by the SEP should not lead to a significant increase in the ratio of the total magnetic fluctuation intensity relative to the background magnetic field.

If $j_g \propto P^{-2\alpha}$, then from equation (11), we see that the wave growth rate γ varies roughly like $k^{2\alpha-2}$. Thus with $\alpha > 1.35$ and

$$I_+^h = I_0\left(\frac{k}{k_0}\right)^{-3/2}\left(\frac{r_0}{r}\right)^3\left(\frac{V + V_{A0}\, r_0/r}{V + V_{A0}}\right)^{-5/2},$$

in $k_L \le k \le k_U$, with $I_0 = 1 \times 10^3$ MeV cm^{-2}, $k_0 = 3.46 \times 10^{-10}(r_0/r)^2$ cm^{-1}, $k_L = 1.46 \times 10^{-10}(r_0/r)^2$ cm^{-1}, $k_U = 5.17 \times 10^{-9}(r_0/r)^2$ cm^{-1}, $V_{A0} = 1 \times 10^{-3}$ AU hr^{-1} and $r_0 = 1$ AU, the growth of wave energy in $(0, k_L)$ is at most comparable to the growth of wave energy in (k_L, k_U), and we can use the increase in the latter as an estimate of the increase in the total wave energy. Since $B = B_0(r_0/r)^2$, where $B_0 = 5 \times 10^{-5}$ G, we estimate the ratio of the *initial* wave intensity in (k_L, k_U) relative to B^2:

$$\frac{\langle(\delta B)^2\rangle_{LU}}{B^2} \approx 1.1 \times 10^{-3}\left(\frac{r}{r_0}\right)^2\left(\frac{V + V_A}{V + V_{A0}}\right)^{-5/2},$$

which varies from 5×10^{-6} at $r = 0.125$ AU to 1.1×10^{-3} at $r = 1$ AU. This shows that the initial wave distribution may be amplified by the low-energy protons through several orders of magnitude at $r < 0.3$ AU and still gives an increase in $\langle(\delta B)^2\rangle$ much less than B^2. We can understand this as follows: at low frequencies there are few high-energy protons to excite the waves, and at high frequencies there is little wave fluctuation to begin with.

3. The model considers only quasi-linear resonant interaction between the particles and parallel and antiparallel Alfvén waves. The treatment of proton transport across the resonance gap in μ (resulting from the upper cutoff wavenumbers for the parallel hydromagnetic Alfvén waves) is oversimplified. Oblique Alfvén waves, wave modes of higher frequencies, e.g., ion cyclotron and magnetosonic waves, and nonresonant scattering can scatter protons in the resonance gap (Jaekel & Schlickeiser 1992; Fisk et al. 1974; Davila & Scott 1984; Smith 1992), and nonlinear theories (e.g., Jones et al. 1973; Völk 1973; Goldstein 1976; Yoon et al. 1991; Karimabadi et al. 1992) do allow the protons to cross the gap. However, it is beyond the scope of the present model to include wave modes with complicated dispersion relations or to treat nonresonant wave-particle interaction and resonance broadening self-consistently. The phenomenological filling of the resonant gap with the average of the $D_{\mu\mu}$ values just outside the gap makes the present model tractable. If this procedure overestimates the effective value of $D_{\mu\mu}$ in the resonance gap, then it also overestimates the μ-diffusion, which will lead to a smaller $\partial f/\partial\mu$, and hence slower growth of the wave intensity and $D_{\mu\mu}$ itself. Thus, in a sense, the error is self-correcting. Nevertheless, a realistic model of wave-particle interaction must treat the above issues rigorously, and this is a challenging task for the future. Bieber & Matthaeus (1992) have recently introduced the concept of dynamical turbulence together with the decay of its correlation function in time. The filling in procedure here is roughly equivalent to assuming a constant turbulence geometry during the course of the particle-driven wave evolution.

4. Large SEP events tend to be gradual and associated with traveling interplanetary shocks (Cane et al. 1988). To model this, we need to inject the SEP at or near the *moving* shock front, and to take account of the first- and second-order Fermi acceleration and adiabatic deceleration via the momentum transport terms. Such work is being undertaken.

The present model suggests that the effective mean free path of ~1 MeV protons decreases with increasing size of the impulsive event, *if* the initial mean free path is small enough to place the observer in the diffusive regime. However, such an anticorrelation will not be found if the initial mean free path is large, is less probable at smaller heliocentric distances because of focusing, and is not expected for high-energy protons. It is not surprising therefore that Wanner & Wibberenz (1993) did not find the above anticorrelation in their study of eight SEP events, five of which were at ≤ 0.65 AU, and all at energies >4 MeV. Kurt, Logachev, & Pissarenko (1977) reported such an anticorrelation for nonrelativistic electrons, whereas Kallenrode, Wibberenz, & Hucke (1992) did not find it in their study of a number of ~0.5 MeV electrons. However, the electrons in these studies have much lower rigidities and do not interact with the Alfvén waves, hence the predictions of our model are not directly applicable to these electrons.

A key prediction of the model is the increased magnetic fluctuations in association with the arrival of intense fluxes of anisotropic solar energetic particles. Are there any observation in support of this prediction? In considering this question, one should bear in mind the clear evidence for the analogous association predicted by Lee (1983) between increased magnetic fluctuations and low-energy ions upstream of traveling interplanetary shocks (e.g., Tsurutani, Smith, & Jones 1983; Viñas, Goldstein, & Acuña 1984; Kennel et al. 1986; Tan et al. 1989).

Beeck et al. (1990) reported an IMF power spectral density that increased by more than an order of magnitude over 1 day for the 1981 July 20 SEP event observed on ISEE3 at 1 AU (their Fig. 11, field data from E. J. Smith and B. T. Tsurutani). They noted that the increase in fluctuations could be generated by the SEP as suggested by Reames (1989). Wanner & Wibberenz (1993) presented a time series of the total power of IMF fluctuations in the wavenumber range 10^{-9}–10^{-8} cm^{-1} for the 1976 March 28 event observed aboard *Helios 2* at 0.5 AU (their Fig. 4, field data from F. M. Neubauer). The total power increased by a factor of 3 early in the event, in agreement with the present model. At present, one would not expect to find much evidence in the published works, since very few correlate in detail SEP observations with IMF power spectrum. According to the model, the chances of observing SEP-driven wave growth increase with event size and decrease strongly with distance from the Sun, and >10 MeV protons contribute negligibly to wave growth because of their relatively small number. Beeck et al.'s observation on the growth of the magnetic power spectral density at 1 AU thus appears remarkable despite the large size of the 1981 July 20 event. However, the interplanetary shock in this event (and most large events) provides a continuously moving particle source that approaches the observer, thus mitigating the strong radial dependence in the present model, which assumes a solar source.

The correlation between the arrival of the SEP and the

growth of the IMF fluctuations in the observations of Beeck et al. and Wanner & Wibberenz may be fortuitous. More observations and careful analyses, using complementary field and particle data on a large number of events, are required to prove the existence of SEP-driven wave growth, and to determine its radial dependence and, most important, the relationship between the time histories of the SEP spectrum and the IMF fluctuation spectrum. Detailed observations of this relationship may prove to be the key to understanding the well-known discrepancy between the theoretical mean free paths calculated from measured IMF power spectra using quasi-linear theory and the mean free paths fitted to observed SEP intensity histories. Because in many events, a substantial fraction of the observed fluctuations appears to be in modes that do not scatter outbound SEP, we caution that the SEP-driven wave growth in such events may be "diluted" by these noninteracting background fluctuations.

While the model is grossly simplified in some respects, it shows that the amplification of interplanetary Alfvén waves by the SEP introduces many interesting features not present in models that assume a time-independent scattering medium. We hope this paper will stimulate more experimental studies on the interactions between interplanetary waves and solar energetic particles using complementary particle and field data, as well as more theoretical work, e.g., inclusion of particle momentum transport, other wave modes, rigorous treatment of pitch diffusion across the resonance gap, traveling interplanetary shock, and comparison between theories and observations.

We thank J. A. Miller, R. Schlickeiser, A. F. Viñas, T. T. von Rosenvinge, and G. Wibberenz for valuable discussions, and M. Peters and S. Walker for software and hardware support. The referee's constructive criticism is greatly appreciated. C. K. N. thanks his co-author and T. T. von Rosenvinge for their hospitality. This work is supported in part by RMIT grant 41123970 and by Universities Space Research Association.

REFERENCES

Barnes, A. 1979, in Solar System Plasma Physics, ed. E. N. Parker, C. F. Kennel, & L. J. Lanzerotti, Vol. 2 (New York: North Holland), 249
———. 1992, J. Geophys. Res., 97, 12105
Bavassano, B., Dobrowolny, M., Mariano, F., & Ness, N. F. 1982, J. Geophys. Res., 87, 3617
Beeck, J., Mason, G. M., Hamilton, D. C., Wibberenz, G., Kunow, H., Hovestadt, D., & Klecker, B. 1987, ApJ, 322, 1052
Beeck, J., Mason, G. M., Marsden, R. G., Hamilton, D. C., & Sanderson, T. R. 1990, J. Geophys. Res., 95, 10279
Bieber, J. W., & Matthaeus, W. H. 1992, in Particle Acceleration in Cosmic Plasmas, ed. G. P. Zank & T. K. Geisser (New York: AIP), 86
Book, D. L., Boris, J. P., & Hain, K. 1975, J. Comput. Phys., 18, 248
Bruno, R., & Bavassano, B. 1991, J. Geophys. Res., 96, 7841
Cane, H. V., Reames, D. V., & von Rosenvinge, T. T. 1988, J. Geophys. Res., 93, 9555
Davila, J. M., & Scott, J. S. 1984, ApJ, 285, 400
Denskat, K. U., & Neubauer, F. M. 1982, J. Geophys. Res., 87, 2215
Earl, J. A. 1974, ApJ, 188, 379
———. 1976, ApJ, 206, 301
———. 1989, ApJ, 343, 936
Feit, J. 1973, Sol. Phys., 29, 211
Fisk, L. A., Goldstein, M. L., Klimas, A. J., & Sandri, G. 1974, ApJ, 190, 417
Forman, M. A., Ramaty, R., & Zweibel, E. G. 1986, in Physics of the Sun, ed. P. A. Sturrock, Vol. 2 (Dordrecht: Reidel), 249
Goldstein, M. L. 1976, ApJ, 204, 900
Hamilton, D. C. 1977, J. Geophys. Res., 82, 2157
Hollweg, J. V. 1974, J. Geophys. Res., 79, 1539
Jaekel, U., & Schlickeiser, R. 1992, J. Phys. G. Nucl. Part. Phys., 18, 1089
Jones, F. C., Kaiser, T. B., & Birmingham, T. J. 1973, Phys. Rev. Lett., 31, 485
Kallenrode, M.-B., Wibberenz, G., & Hucke, S. 1992, ApJ, 394, 351
Karimabadi, H., Krauss-Varban, D., & Terasawa, T. 1992, J. Geophys. Res., 97, 13853
Kennel, C. F., Coroniti, F. V., Scarf, F. L., Livesey, W. A., Russel, C. T., Smith, E. J., Wenzel, K.-P., & Scholer, M. 1986, J. Geophys. Res., 91, 11917
Kurt, V. G., Logachev, Yu. I., & Pissarenko, N. F. 1977, Sol. Phys., 53, 157
Lee, M. A. 1971, Plasma Phys., 13, 1079
———. 1972, ApJ, 178, 837
———. 1982, J. Geophys. Res., 87, 5063
———. 1983, J. Geophys. Res., 88, 6109
———. 1988, in Plasma Waves and Instablities at Comets and in Magnetospheres, ed. B. T. Tsurutani & O. Hiroshi (Washington, DC: AGU), 13
Lee, M. A., & Ip, W.-H. 1987, J. Geophys. Res., 92, 11041
Lee, M. A., & Ryan, J. M. 1986, ApJ, 303, 829
Marsch, E. 1991, in Physics of the Inner Heliosphere, ed. R. Schwenn & E. Marsch, Vol. 2 (Berlin: Springer), 159
Marsch, E., & Tu, C.-Y. 1990, J. Geophys. Res., 95, 8211
Mason, G. M., Ng, C. K., Klecker, B., & Green, G. 1989, ApJ, 339, 529
McCracken, K. G., Rao, U. R., Bukata, R. P., & Keath, E. P. 1971, Sol. Phys., 18, 100
McGuire, R. E., & von Rosenvinge, T. T. 1984, Adv. Space Res., 4, 117
McGuire, R. E., von Rosenvinge, T. T., & McDonald, F. B. 1981, Proc. 17th Internat. Cosmic Ray Conf. (Paris), 3, 65
Melrose, D. B. 1980, Plasma Astrophysics, Vol. 1 (New York: Gordon & Breach)
Miller, J. A. 1991, ApJ, 376, 342
Ng, C. K., Wibberenz, G., Green, G., & Kunow, H. 1983, Proc. 18th Internat. Cosmic Ray Conf. (Bangalore), 381
Ng, C. K., & Wong, K. Y. 1979, Proc. 16th Internat. Cosmic Ray Conf. (Kyoto), 5, 252
Omura, Y., & Matsumoto, H. 1989, in Plasma Waves and Instabilities at Comets and in Magnetospheres, ed. B. T. Tsurutani & O. Hiroshi (Washington, DC: AGU), 51
Palmer, I. D. 1982, Rev. Geophys. Space Phys., 20, 335
Parker, E. N. 1963, Interplanetary Dynamical Processes (New York: Interscience)
Reames, D. V. 1989, ApJ, 342, L51
———. 1990, ApJ, 358, L63
———. 1992, in Eruptive Solar Flares, ed. Z. Svestka, B. V. Jackson, & M. E. Machado (New York: Springer), 180
———. 1993, Adv. Space Res., 13, 331
Reames, D. V., Richardson, I. G., & Wenzel, K.-P. 1992, ApJ, 387, 715
Richardson, I. G., Reames, D. V., Wenzel, K.-P., & Rodriguez-Pacheco, J. 1990, ApJ, 363, L9
Roberts, D. A., & Goldstein, M. L. 1991, Rev. Geophys. Suppl., 29, 932
Roberts, D. A., Goldstein, M. L., & Klein, L. W. 1990, J. Geophys. Res., 95, 4203
Roelof, E. C. 1969, in Lectures in High-Energy Astrophysics, ed. H. Ogelman & J. R. Wayland (Washington, DC: NASA SP-199), 111
Schlickeiser, R. 1989a, ApJ, 336, 243
———. 1989b, ApJ, 336, 264
Smith, C. W. 1992, in Particle Acceleration in Cosmic Plasmas, ed. G. P. Zank, & T. K. Geisser (New York: AIP), 79
Stix, T. H. 1962, The Theory of Plasma Waves (New York: McGraw-Hill)
Tademaru, E. 1969, ApJ, 158, 959
Tan, L. C., Mason, G. M., Gloeckler, G., & Ipavich, F. M. 1989, J. Geophys. Res., 94, 6552
Tsurutani, B. T., Smith, E. J., & Jones, D. E. 1983, J. Geophys. Res., 88, 5645
Tu, C.-Y., Pu, Z.-Y., & Wei, F.-S. 1984, J. Geophys. Res., 89, 9695
Van Hollebeke, M. A. I., McDonald, F. B., & Meyer, J. P. 1990, ApJS, 73, 285
Viñas, A. F., Goldstein, M. L., & Acuña, M. H. 1984, J. Geophys. Res., 89, 3762
Völk, H. J. 1973, Ap&SS, 25, 471
———. 1975, Rev. Geophys. Space Phys., 13, 4
Wanner, W., & Wibberenz, G. 1993, J. Geophys. Res., 98, 3513
Webb, S., Balogh, A., Quenby, J. J., & Sear, J. F. 1973, Sol. Phys., 29, 477
Whang, Y. C. 1973, J. Geophys. Res., 78, 7221
Wong, K. Y. 1982, M.Sc. thesis, Univ. of Malaya.
Wu, C. S., & Davidson, R. C. 1972, J. Geophys. Res., 77, 5399
Yoon, P. H., Ziebell, L. F., & Wu, C. S. 1991, J. Geophys. Res., 96, 5469
Zwickl, R. D., & Webber, W. R. 1977, Sol. Phys., 54, 457